Circulation
JOURNAL OF THE AMERICAN HEART ASSOCIATION

Therapeutic Inhibition of miR-208a Improves Cardiac Function and Survival During Heart Failure

Rusty L. Montgomery, Thomas G. Hullinger, Hillary M. Semus, Brent A. Dickinson, Anita G. Seto, Joshua M. Lynch, Christianna Stack, Paul A. Latimer, Eric N. Olson and Eva van Rooij

Circulation. 2011;124:1537-1547; originally published online September 6, 2011;
doi: 10.1161/CIRCULATIONAHA.111.030932
Circulation is published by the American Heart Association, 7272 Greenville Avenue, Dallas, TX 75231

Print ISSN: 0009-7322. Online ISSN: 1524-4539

Therapeutic Inhibition of miR-208a Improves Cardiac Function and Survival During Heart Failure

Rusty L. Montgomery, PhD; Thomas G. Hullinger, PhD; Hillary M. Semus, MS; Brent A. Dickinson, BS; Anita G. Seto, PhD; Joshua M. Lynch, BS; Christianna Stack, MS; Paul A. Latimer, BS; Eric N. Olson, PhD; Eva van Rooij, PhD

Background—Diastolic dysfunction in response to hypertrophy is a major clinical syndrome with few therapeutic options. MicroRNAs act as negative regulators of gene expression by inhibiting translation or promoting degradation of target mRNAs. Previously, we reported that genetic deletion of the cardiac-specific miR-208a prevents pathological cardiac remodeling and upregulation of Myh7 in response to pressure overload. Whether this miRNA might contribute to diastolic dysfunction or other forms of heart disease is currently unknown.

Methods and Results—Here, we show that systemic delivery of an antisense oligonucleotide induces potent and sustained silencing of miR-208a in the heart. Therapeutic inhibition of miR-208a by subcutaneous delivery of antimiR-208a during hypertension-induced heart failure in Dahl hypertensive rats dose-dependently prevents pathological myosin switching and cardiac remodeling while improving cardiac function, overall health, and survival. Transcriptional profiling indicates that antimiR-208a evokes prominent effects on cardiac gene expression; plasma analysis indicates significant changes in circulating levels of miRNAs on antimiR-208a treatment.

Conclusions—These studies indicate the potential of oligonucleotide-based therapies for modulating cardiac miRNAs and validate miR-208 as a potent therapeutic target for the modulation of cardiac function and remodeling during heart disease progression. **(*Circulation*. 2011;124:1537-1547.)**

Key Words: gene expression regulation ■ heart failure ■ hypertension ■ hypertrophy ■ microRNAs ■ molecular biology ■ ventricular remodeling

Chronic and acute stress to the heart results in a pathological remodeling response accompanied by cardiomyocyte hypertrophy, fibrosis, pump failure, myocyte degeneration, and apoptosis, which often culminate in heart failure and sudden death.[1] Although classic pharmacological treatment strategies can reduce remodeling and prolong survival in heart failure patients, these therapies are ultimately ineffective in preventing progression of the disease. A hallmark of pathological hypertrophy and heart failure is the reactivation of a set of fetal cardiac genes, including those encoding atrial natriuretic factor, B-type natriuretic peptide, and fetal isoforms of contractile proteins such as skeletal α-actin and Myh7 (β-myosin heavy chain).[2] Downregulation of Myh6 (α-myosin heavy chain) and upregulation of Myh7 are common responses to cardiac injury regardless of the species.[3–5] Relatively minor increases in the ratio of Myh6 to Myh7 have been shown to have beneficial effects on cardiac contractility and performance in humans and rodents.[6–8]

Clinical Perspective on p 1547

Previously, we and others identified signature expression patterns of microRNAs (miRNAs) associated with pathological cardiac hypertrophy, heart failure, and myocardial infarction in humans and in mouse models of heart disease (reviewed elsewhere[9]). Gain- and loss-of-function studies in mice have revealed profound and unexpected functions for these miRNAs in numerous facets of cardiac biology, including the control of myocyte growth, contractility, and fibrosis (reviewed by Montgomery et al[10]). Especially intriguing is miR-208, an miRNA encoded within an intron of the *Myh6* gene, which regulates the cardiac stress response.[11,12] Although genetic deletion of miR-208 in mice failed to induce an overt phenotype at baseline, in response to several forms of cardiac stress, miR-208–null mice showed virtually no cardiomyocyte hypertrophy or fibrosis and were unable to upregulate Myh7 expression.[11,12]

In the adult heart, miR-208 is essential for the expression of not only Myh7, but also a closely related myosin isoform,

Received March 9, 2011; accepted August 11, 2011.

From miRagen Therapeutics, Boulder, CO (R.L.M., T.G.H., H.M.S., B.A.D., A.G.S., J.M.L., C.S., P.A.L., E.v.R.), and Department of Molecular Biology, University of Texas Southwestern Medical Center, Dallas (E.N.O.).

The online-only Data Supplement is available with this article at http://circ.ahajournals.org/lookup/suppl/doi:10.1161/CIRCULATIONAHA.111.030932/-/DC1.

Correspondence to Eva van Rooij, PhD, miRagen Therapeutics, Inc, Boulder, CO 80301. E-mail evanrooij@miragenrx.com

Circulation **is available at http://circ.ahajournals.org** **DOI: 10.1161/CIRCULATIONAHA.111.030932**

Myh7b.[12,13] Remarkably, both of these genes encode slow myosins and contain intronic miRNAs (miR-208b and miR-499, respectively).[14,15] Because miR-208 (called miR-208a here), miR-208b, and miR-499 are related miRNAs that arise from myosin genes, we collectively refer to these miRNAs as MyomiRs.[16] Through gain- and loss-of-function experiments in mice, we have shown that genetic deletion of miR-208a dose-dependently reduces Myh7b/miR-499 expression within the adult heart.[13] Because miR-499–mutant animals show no effect on Myh7 expression or cardiac remodeling in response to stress and reintroduction of miR-499 removes the cardiac effects seen in the miR-208a–mutant mice,[13] we conclude that the combined reduction in miR-208a and miR-499 is responsible for the cardioprotective effects seen in miR-208a–mutant animals.

The importance of miRNAs for cardiac function and dysfunction suggests opportunities for therapeutically exploiting the biology of miRNAs in the setting of heart disease. Single-stranded oligonucleotides have been shown to be effective in inactivating miRNAs in vivo[17–21] and represent a potentially effective means of inactivating pathological miRNAs. Here, we show that systemic delivery of locked nucleic acid (LNA)–modified antisense oligonucleotides against miR-208a is sufficient to induce specific, potent, and sustained silencing of miR-208a in the heart. Moreover, antimiR-208a dose-dependently blunts stress-induced remodeling, functional deterioration, and cardiac myosin switching while improving general health and survival in a rat model of diastolic heart failure (Dahl salt-sensitive rats). Gene expression analysis showed specific gene expression changes in response to antimiR-208a treatment, including changes in previously defined target genes. Intriguingly, these physiological effects of antimiR-208a in hypertensive rats are mirrored by significant changes in plasma levels of circulating miRNAs. Together, these studies indicate the potency of systemically delivered anti-miRs in the settings of heart disease and validate miR-208 as an important therapeutic target during heart failure.

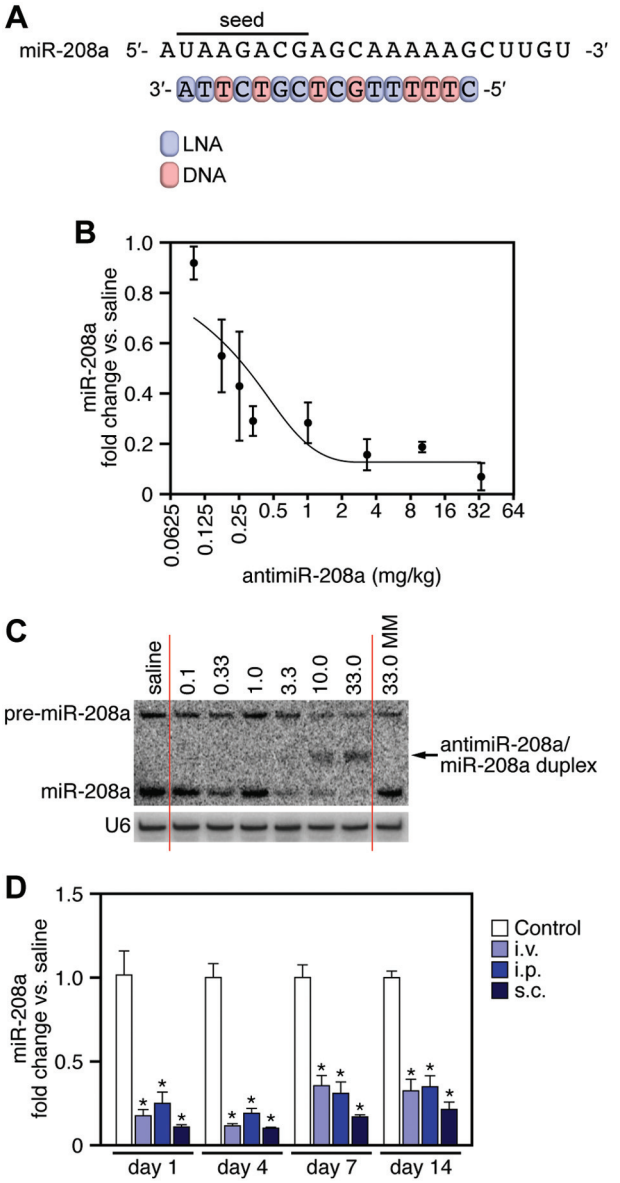

Figure 1. Systemic delivery of antimiR-208a induces potent and sustained silencing of miR-208 in the heart. **A**, Locked nucleic acid (LNA)–modified antisense oligonucleotide chemistry directed against the 5′end of miR-208a (antimiR-208a). **B**, Real-time polymerase chain reaction analysis on murine hearts 1 week after intravenous delivery of increasing doses of antimiR-208a shows a dose-dependent reduction in miR-208a levels. **C**, Northern blot analysis on total RNA from murine hearts 1 week after intravenous delivery of antimiR-208a shows a dose-dependent reduction in miR-208a detection, whereas a control mismatch chemistry (MM) has no effect on miR-208a. U6 serves as a loading control. **D**, Real-time polymerase chain reaction analysis on cardiac tissue collected at the indicated time points shows that intravenous, intraperitoneal, or subcutaneous delivery of 25 mg/kg antimiR-208a induces potent silencing of miR-208a. In **B** and **D**, error bars depict SEM (n=4 for each time point and dose).

Methods

Animal Procedures

All animal protocols were approved by the Institutional Animal Care and Use Committee of miRagen Therapeutics, Inc.

Animals and Delivery of Locked Nucleic Acid–Modified Anti-miRs

The LNA–anti-miR oligonucleotides were synthesized at miRagen Therapeutics, Inc. as fully phosphorothiolated oligonucleotides perfectly complementary to the 5′ region of the mature miR-208a sequence. For the dose response in Figure 1, a mismatch antimiR-208a control was used that contained 3-bp mismatches (5′-CtttGTgCtCGtAtGA-3′; upper case indicates LNA; lower case, DNA). For all subsequent experiments, we used a universal control with identical chemistry. This LNA control oligonucleotide consisted of a sequence directed against a *Caenorhabditis elegans*–specific miRNA (5′-TccTAgAAaGAgtAgA-3′; upper case indicates LNA; lower case, DNA). Unless indicated otherwise, in vivo delivery of the oligonucleotide chemistries was achieved by low-pressure intravenous injections via the tail vein of either adult male C56Bl6 mice or adult male Dahl salt-sensitive rats (Harlan, Indianapolis). All chemistries were dissolved and injected in a comparable end volume of saline, after which the animals were examined for obvious side effects of the chemistries. Tissue samples were collected at the indicated time points for molecular or histological examination. Dahl rats were maintained on 0.25 NaCl or placed on 4% or 8% NaCl diet at 8 weeks of age (Harlan, Indianapolis, IN).

Quantitative Real-Time Polymerase Chain Reaction Analysis

For in vivo real-time polymerase chain reaction (RT-PCR) analysis, RNA was extracted from cardiac tissue with Trizol (Invitrogen); then, 2 μg RNA from each tissue sample was used to generate cDNA with Super Script II reverse transcriptase according to the manufacturer's specifications (Invitrogen). To detect the level of miR-208, RT-PCR was performed with the Taqman MicroRNA assay (Applied Biosystems, ABI) according to the manufacturer's recommendations, using 10 to 100 ng total RNA. The expression of a subset of genes was analyzed by quantitative RT-PCR with Taqman probes purchased from ABI.

Northern Blot Analysis

Total RNA was isolated from cardiac tissue samples by the use of Trizol reagent (Gibco/BRL). Northern blots to detect microRNAs were performed as described previously. A U6 probe served as a loading control (IDT). Total RNA (10 μg) from cardiomyocytes or heart tissue was loaded onto 20% acrylamide denaturing gels and transferred to Zeta-probe GT genomic blotting membranes (Bio-Rad) by electrophoresis. After transfer, the blots were cross-linked and baked at 80°C for 1 hour. To maximize the sensitivity of miRNA detection, oligonucleotide probes were labeled with the Starfire Oligos Kit (IDT, Coralville, IA) and α-^{32}P dATP (Amersham or Perkin Elmer). Probes were hybridized to the membranes overnight at 39°C in Rapid-hyb buffer (Amersham); afterward, they were washed twice for 10 minutes at 39°C with 0.5× saline-sodium citrate containing 0.1% SDS. The blots were exposed and quantified by PhosphorImager analysis (GE HealthCare Life Sciences), and a U6 probe served as a loading control (ABI). The intensity of the radioactive signal was used to quantify the fold change in expression with a PhosphorImager and ImageQuant (Bio-Rad).

Western Blot Analysis

For Western blot analysis, myosin was extracted from cardiac cells or tissue as described.[22] Myosin heavy chain isoforms were detected by loading 0.1 μg protein lysate on a 4% to 15% gradient gel and separated by SDS-PAGE, and Western blotting was performed with mouse monoclonal anti-myosin (slow, skeletal M8421; Sigma, MO), which is highly specific for Myh7.

Biodistribution Assay

A sandwich hybridization assay was used to quantify antimiR-208a in plasma and tissue samples. Probes for the hybridization assay were synthesized with 2′Ome and LNA-modified nucleotides and are bTEG-mU;lA;mA;lG;mA;lC;mG (capture probe) and mA;lG;mC;lA;mA;lA;mA;lA;mG-6FAM (detection probe). Detection was accomplished with anti-fluorescence–peroxidase, Fab fragments (Roche), and TMB Peroxidase Substrate (KPL). Standard curves were generated with nonlinear logistic regression analysis with 4 parameters (4-PL). The working concentration range of the assay was 2 to 536 ng/mL. Tissue samples were prepared at 100 mg/mL by homogenizing in 3 mol/L GITC buffer (3 mol/L guanidine isothiocyanate, 0.5 mol/L NaCl, 0.1 mol/L Tris, pH 7.5, and 10 mmol/L EDTA) 2 times for 30 seconds with an MP FastPre-24 at a speed setting of 6.0. Plasma samples and tissue homogenates were diluted a minimum of 50-fold in 1 mol/L GITC Buffer (1 mol/L guanidine isothiocyanate, 0.5 mol/L NaCl, 0.1 mol/L Tris, pH 7.5, and 10 mmol/L EDTA) for testing.

Echocardiography

Cardiac function was evaluated by 2-dimensional transthoracic echocardiography on sedated rats (2%–2.5% isoflurane) using a Visual Sonic Ultrasound system with a 30-MHz transducer. The heart was imaged in a parasternal short-axis view at the level of the papillary muscles to record M-mode measurements and to determine heart rate, wall thickness, and end-diastolic and end-systolic dimensions. Fractional shortening (defined as the end-diastolic dimension minus the end-systolic dimension normalized for the end-diastolic dimension) was used as an index of cardiac contractile function. Diastolic function was assessed with transmitral flow Doppler from an apical 4-chamber view to measure the E/A ratio, isovolumic relaxation time, and deceleration time of E-wave velocity.

Surface ECG Measurement

Mice were anesthetized with 2% isoflurane in 200 mL/min O_2, and rats were anesthetized with 2% isoflurane in 500 mL/min breathing air via nosecone. Body temperature for mice and rats was maintained at 37° to 38°C with a Homeothermic Warming System (Kent Scientific) or a heat lamp and warming platform (Visual Sonics). Lead II ECGs were recorded for 10 minutes with subcutaneous needle electrodes and an Iworx data acquisition system sampling at 1 kHz. Using Labscribe software (Iworx), we analyzed tracings after 2, 4, 6, 8, and 10 minutes and inspected them for normal sinus rhythm; ≈40 beats at each time point were analyzed by the use of computerized techniques to quantify signal intervals (HR, PR, QRS, QT, and QTc).

Histology

Tissues used for histology were incubated in Krebs-Henseleit solution, fixed in 4% paraformaldehyde, sectioned, and processed for hematoxylin and eosin and Picrosirius Red staining or in situ hybridization by standard techniques.[23] Images of ≈100 cardiomyocytes per animal in cross section were captured from the hematoxylin and eosin–stained sections. Cardiomyocyte cross-sectional areas were measured with Image-Pro Plus software, and a mean was determined for each animal. Perivascular fibrosis images were taken from epicardial, mid, and endocardial regions from the Picrosirius Red–stained sections from each animal. Image-Pro plus software was used to determine the total vessel wall area, including perivascular fibrosis. The luminal area was subtracted from the total vessel wall area. Perivascular fibrosis was determined via color segmentation and reported as percent of the total vessel wall area.

Gene Expression Analysis

Microarray profiling was performed on Illumina RatRef-12 BeadChip arrays by a service provider (Expression Analysis, Durham, NC). Total RNA was isolated from cardiac tissue as described above. Analysis of differential gene expression was performed by the service provider using permutation analysis of differential expression. Note that if a gene probe does not have detection value of $P \leq 0.05$ in all 12 arrays, then that gene is omitted from subsequent analysis. Differential expression graphs were provided by the service provider. Gene clustering was performed with Cluster 3.0, and heat map images were generated in Java TreeView. Gene ontology was performed with the online tool found at www.pantherdb.org. Predicted miR-208 gene targets in the rat were found with www.targetscan.org (TargetScan), www.pictar.mdc-berlin.de (Pictar), and www.microrna.org (miRanda). Of all the gene targets predicted by miRanda, only those with an mirsvr score of < -0.1 were included in the analysis. For the identification of miR-208 targets, a cutoff value for differential expression of $P \leq 0.05$ was used.

Quantitative Real-Time Polymerase Chain Reaction Analysis From Plasma

RNA from plasma samples was isolated with Trizol LS Reagent (Invitrogen) following the manufacturer's protocol. Before RNA isolation, we added 250 pmol of 2 different synthetic *C. elegans* miRNA sequences to serve as internal controls for normalization of target miRNAs. The *C. elegans* sequences used were cel-miR-2 (UAUCACAGCCAGCUUUGAUGUGC) and cel-lin-4 (UCCCUGAGACCUCAAGUGUGA) (Dharmacon). The final RNA pellet was resuspended in a final volume equal to the initial plasma volume, and 5 μL was used for subsequent RT-PCR reactions, as described above.

Statistical Analysis

One-way ANOVA and the Newman-Keuls multiple comparison post test were used to determine significance. Values of $P<0.05$ were considered statistically significant. For the Kaplan-Meier survival curve, a Mantel-Cox log-rank test was used to determine significance.

Results

Anti-miR–Mediated Silencing of miR-208a In Vivo

To determine the therapeutic potential of miR-208a inhibition in cardiomyocytes in vivo, we designed an LNA-containing anti-miR targeting bases 2 to 17 of the 5′ region of mature miR-208a and containing a combination of LNA and DNA linked by phosphorothioate bonds (Figure 1A). RT-PCR and Northern blot analysis 1 week after intravenous delivery of antimiR-208a at doses ranging from 0.1 to 33 mg/kg indicated the dose-responsive silencing of miR-208a, whereas injection of a mismatch anti-miR of similar chemistry showed no inhibition of miR-208a (Figure 1B and 1C). Notably, we observed an upshift of miR-208 in the presence of antimiR-208a, reflecting the formation of a stable heteroduplex between miR-208a and the LNA anti-miR. Real-time analysis of the other 2 MyomiRs, miR-208b and miR-499, showed no inhibition after a single injection after 7 days, nor did we observe any changes in Myh7 (data not shown).

To investigate the potential to deliver antimiR-208a via additional routes of administration, we compared miR-208a inhibition after injection of mice intravenously, intraperitoneally, or subcutaneously with 25 mg/kg antimiR-208a. All 3 routes of administration showed robust inhibition of miR-208a at days 1, 4, 7, and 14 (Figure 1D), with no significant differences in antimiR-208a detection between the different delivery methods for plasma, heart, liver, or kidney (Figure I in the online-only Data Supplement).

Prolonged miR-208a Inhibition Leads to Myh7 Regulation In Vivo

Because a single dose of antimiR-208a after 7 days was unable to influence Myh7 expression, we sought to determine the dose and time required for efficient Myh7 regulation after antimiR-208a administration. Three consecutive doses of 33 mg/kg antimiR-208a robustly inhibited miR-208a for at least 6 weeks (Figure 2A). miR-499, which is regulated by miR-208,[13] showed a time-dependent decrease in expression from 1 to 6 weeks after administration of antimiR-208a (Figure 2A). Furthermore, *Myh7* expression was significantly reduced starting 4 weeks after antimiR-208a treatment, suggesting that a specific threshold of miR-208a and miR-499 levels is necessary for *Myh7* expression (Figure 2B), which was paralleled by a reduction in Myh7 protein (Figure 2C). The initial spike in *Myh7* mRNA in response to antimiR-208a is not translated into increased Myh7 protein (Figure 2B and 2C).

To establish whether the effect on Myh7 expression is based on a reduction in both miR-208a and miR-499, we injected mice for 3 consecutive days with a cocktail of antimiR-208a and anti–miR-499, each at 33 mg/kg. Treatment with antimiR-208a/499 caused robust inhibition of miR-208a and miR-499 for 6 weeks and demonstrated a much more rapid regulation of Myh7 mRNA and protein, with reduced expression before 2 weeks after treatment (Figure 2A through 2C). Consistent with its host gene, miR-208b expression showed a downregulation beginning at 4 weeks (Figure II in the online-only Data Supplement). Additionally, we used a universal control oligo with the same modifications for this and all subsequent studies, which showed no effects on miR-208a, miR-208b, miR-499, or Myh7, suggesting that the downregulation is due to specific inhibition of miR-208a (Figure 2A through 2C and Figure II in the online-only Data Supplement). Anti-miR distribution data indicated that considerable amounts of antimiR-208a were still detectable in heart, liver, kidney, and plasma 6 weeks after administration of either 33 mg/kg or 3×33 mg/kg of antimiR-208a (Figure 2D and 2E).

Therapeutic Silencing of miR-208 Reduces Cardiac Remodeling While Improving Cardiac Function and Survival During Heart Failure

We next aimed to test the therapeutic relevance of miR-208a inhibition. To this end, we used Dahl salt-sensitive rats that were fed either a low-salt diet (0.25% NaCl) or a high-salt (HS) diet (8.0% NaCl) starting at 8 weeks of age. Initiation of an HS diet in Dahl salt-sensitive rats results in chronic hypertension, which progresses to a model of congestive heart failure associated primarily with diastolic dysfunction.[24] After 1 week on the HS diet, rats were administered saline, 25 mg/kg antimiR-208a, or 25 mg/kg scrambled control oligo subcutaneously every 2 weeks. After 3 to 4 weeks on the HS diet, the saline- and control-treated animals started to show signs of discomfort and died, whereas subcutaneous delivery of antimiR-208a significantly alleviated these symptoms (Figure 3A). As an indication of health, we monitored body weight during the duration of the study. Dahl rats on the HS diet injected with either saline or the control oligo exhibited significant reductions in weight gain compared with controls on the low-salt diet. The HS/antimiR-208a–treated rats, however, showed comparable weight gain (Figure 3B). To exclude the possibility that antimiR-208a–treated animals were maintaining weight through ingesting less of the 8% HS diet, food intake was monitored, which showed a comparable ingestion between all HS-fed groups (Figure III in the online-only Data Supplement).

To obtain additional insight into the basis for the protective effects seen in response to antimiR-208a, subsequent studies were done with a 4.0% NaCl diet during which the rats received saline, 5 or 25 mg/kg of antimiR-208a, or 25 mg/kg of anti-miR control every 2 weeks. Body weight analysis indicated that Dahl rats on the HS diet exhibited significant reductions in weight gain compared with the controls on the low-salt diet, whereas the HS/antimiR-208a–treated rats maintained their increase in weight gain (Figure 3C). Functional assessment with echocardiography indicated that antimiR-208a–treated rats exhibited a significant dose-dependent reduction in isovolumic relaxation time compared with HS/saline controls, as well as a normalization of the mitral valve early to active filling velocity ratio compared with HS/saline con-

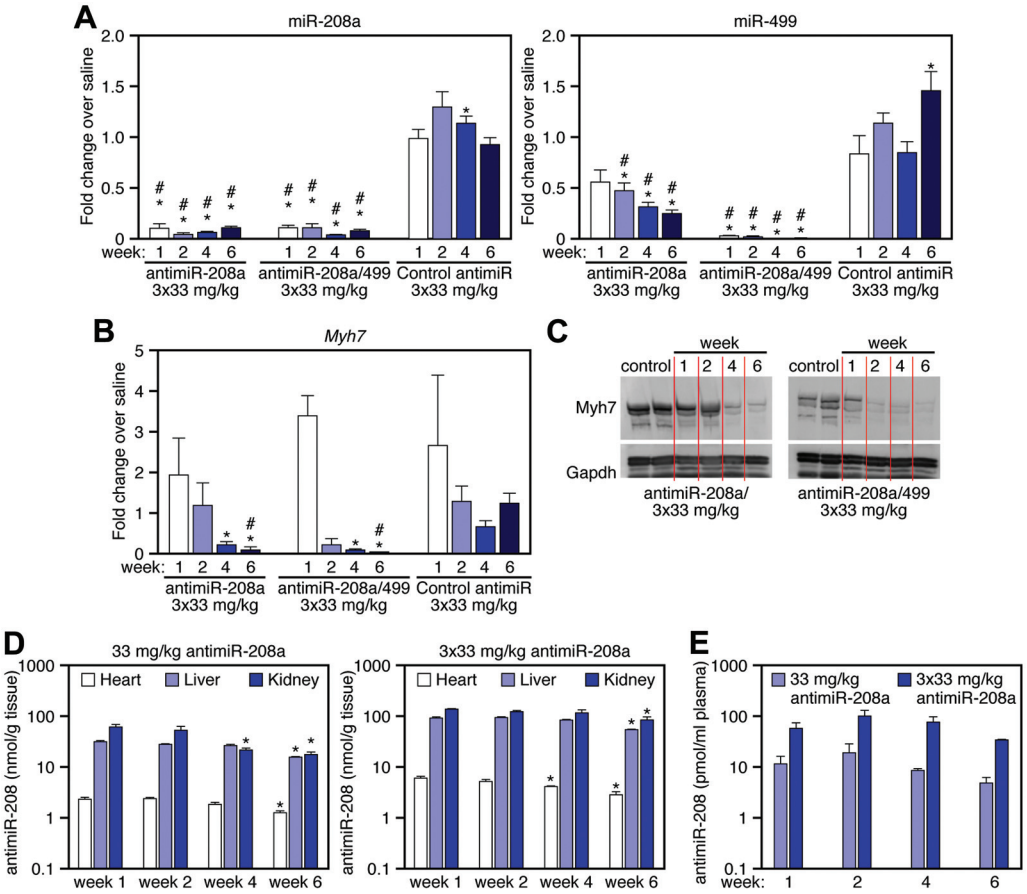

Figure 2. miR-208a silencing reduces miR-499 and Myh7. **A**, Real-time polymerase chain reaction analysis shows that antimiR-208a potently reduces cardiac levels of miR-208a up to 6 weeks after injection, which leads to a time-dependent reduction in miR-499. Dosing with an anti-miR against both miR-208a and miR-499 induces a more rapid reduction in cardiac levels of both miR-208a and miR-499. Control anti-miR shows no robust effect on miR-208a or miR-499 expression. **B**, *Myh7* is reduced 4 weeks after miR-208a inhibition, whereas inhibition of miR-208a and miR-499 reduces *Myh7* after 2 weeks, as shown by real-time polymerase chain reaction. Control anti-miR shows no robust effect on Myh7 expression. **C**, Western blot analysis for Myh7 showing reduced Myh7 expression at the indicated time points after antimiR-208a or antimiR-208a/-499 treatment. GAPDH serves as a loading control. Each lane is a representative animal from **B**. **D** and **E**, Tissue distribution analysis indicates that antimiR-208a is detectable in heart, liver, kidney (**D**), and plasma (**E**) up to 6 weeks after injection. In **A**, **B**, **D**, and **E**, error bars depict the SEM (n=4 for each time point and dose). In **A** and **B**, *$P<0.05$ vs saline at the same time point; #$P<0.05$ vs control anti-miR at the same time point. In **D**, *$P<0.05$ vs week 1 for the same tissue.

trols 8 weeks after the HS diet (Figure 3D and Figure IV in the online-only Data Supplement). Time-dependent echocardiography performed every 2 weeks after the HS diet showed significant reductions in isovolumic relaxation time in antimiR-208a–treated rats compared with HS/saline controls (Figure IV in the online-only Data Supplement). Quantification of cardiomyocyte size showed a significant reduction in cardiomyocyte hypertrophy after treatment with antimiR-208a (Figure 3E and 3F). Additionally, antimiR-208a treatment reduced periarteriolar fibrosis induced by the HS diet as assessed by quantification of Picrosirius Red staining (Figure 3E and 3F).

miR-208a Inhibition Reverses Myosin Switching During Heart Failure

AntimiR-208a caused a dose-dependent inhibition of miR-208a in both left and right ventricles 2 weeks after the last injection with antimiR-208a, whereas a control oligo showed no difference compared with saline (Figure 4A). miR-499 also showed a dose-dependent decrease in expression after sustained inhibition of miR-208a (Figure 4A). miR-208b was induced in both HS/saline– and HS/control–treated animals, paralleling the upregulation of β-myosin heavy chain; however, antimiR-208a treatment resulted in a dose-dependent decrease in miR-208b levels (Figure 4A). This regulation of miR-499 and miR-208b was confirmed by Northern blot analysis (Figure 4B).

To assess the regulation of the myosin host genes, we examined *Myh6*, *Myh7*, and *Myh7b* mRNA levels. *Myh7* was significantly increased in response to HS in both the HS/saline and HS/control groups. This increase was dose-dependently blunted in response to antimiR-208a. Additionally, antimiR-208a treatment normalized the decreased expression of *Myh6* mRNA observed in both the HS/saline and HS/control groups (Figure 4C). Expression of *Myh7b* mirrored miR-499 levels, exhibiting a dose-dependent reduction on antimiR-208a treatment. Furthermore, the dose-dependent regulation of Myh7 was confirmed by

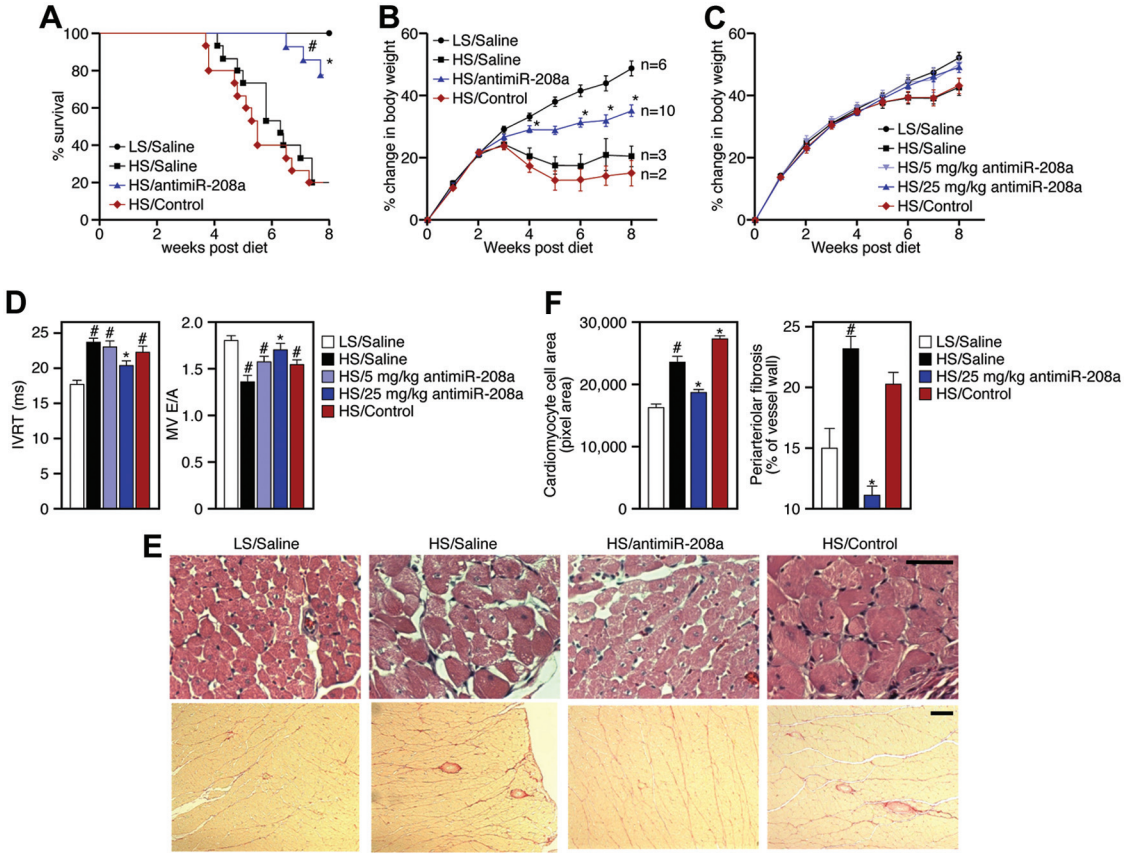

Figure 3. Therapeutic silencing of miR-208a is beneficial during heart failure. **A**, Kaplan-Meier survival curves in the Dahl hypertensive rat model show a pronounced decrease in survival in response to an 8% high-salt (HS) diet for both the HS/saline and HS/control groups, which is significantly improved in response to antimiR-208a treatment. Rats were dosed every 2 weeks at 25 mg/kg starting 1 week after the HS diet. *$P=0.0038$ vs HS/saline; #$P<0.0001$ vs HS/control. **B**, Body weight analysis indicates that Dahl hypertensive rats on an 8% HS diet exhibit reduced weight gain compared with animals on a low-salt (LS) diet, whereas HS/antimiR-208a–treated rats show a significantly better maintenance in weight gain. For **A** and **B**, n=6 for LS/saline; n=15 for HS/saline and HS/control; and n=14 for HS/antimiR-208a. n Indicates total survivors remaining at week 8 after the diet. **C**, Body weight analysis of Dahl rats on the 4% HS diet shows significant reductions in weight gain compared with LS diet controls, whereas both 5- and 25-mg/kg injections every 2 weeks are sufficient to maintain weight gain comparable to that in animals on a normal diet. **D**, Echocardiography measurements indicate that the increase in isovolumic relaxation time (IVRT) and decrease in mitral valve early to active filling velocity ratio (MV E/A) in response to a 4% HS diet are significantly improved in response to antimiR-208a treatment 8 weeks after the start of the diet. For **C** and **D**, n=10 for all groups. **E**, Representative images of hematoxylin and eosin (H&E)– and Picrosirius Red– stained left ventricular histological sections indicate an increase in cardiomyocyte hypertrophy and perivascular fibrosis in response to the 4% HS diet for 8 weeks, whereas both parameters are reduced in response to antimiR-208a treatment. H&E, scale bar=50 μm; Picrosirius Red, scale bar=100 μm. **F**, Bar graph representation of histological quantification showing significantly less hypertrophy and fibrosis in the presence of antimiR-208a. In **D** and **F**, error bars depict the SEM. *$P<0.05$ vs HS/saline; #$P<0.05$ vs LS/saline.

Western blot (Figure 4D). In addition, antimiR-208a treatment resulted in a derepression of the previously characterized miR-208a target, HP1β, further suggesting that antimiR-208a action occurs through miR-208a inhibition (Figure 4E and Figure V in the online-only Data Supplement).

AntimiR-208a Does Not Induce Changes in Cardiac Conductance or Signs of Toxicity

Although genetic deletion of miR-208a does not affect viability or cause gross morphological heart defects, a previous report mentioned that miR-208a might be required for proper heart electrophysiology.[12] To verify whether antimiR-208a treatment resulted in cardiac conductance effects, we measured ECGs in both wild-type mice and diseased rats. Both species showed proper cardiac electrophysiology after antimiR-208a treatment for an extended period of time (Figure VI and Tables I and II in the online-only Data Supplement).

Regardless of the route of administration, all mice and rats tolerated the antimiR-208a or control oligo well and exhibited normal behaviors, as determined by activity level and grooming throughout the study. Compared with saline, antimiR-208a or the control oligo did not induce baseline changes in body or tissue weight up to 6 weeks after dosing (Table III). Neither antimiR-208a nor control oligo treatment changed serum levels of the alanine aminotransferase or aspartate aminotransferase liver enzymes in rats (Figure VII), suggesting that the oligonucleotides do not induce overt liver toxicities.

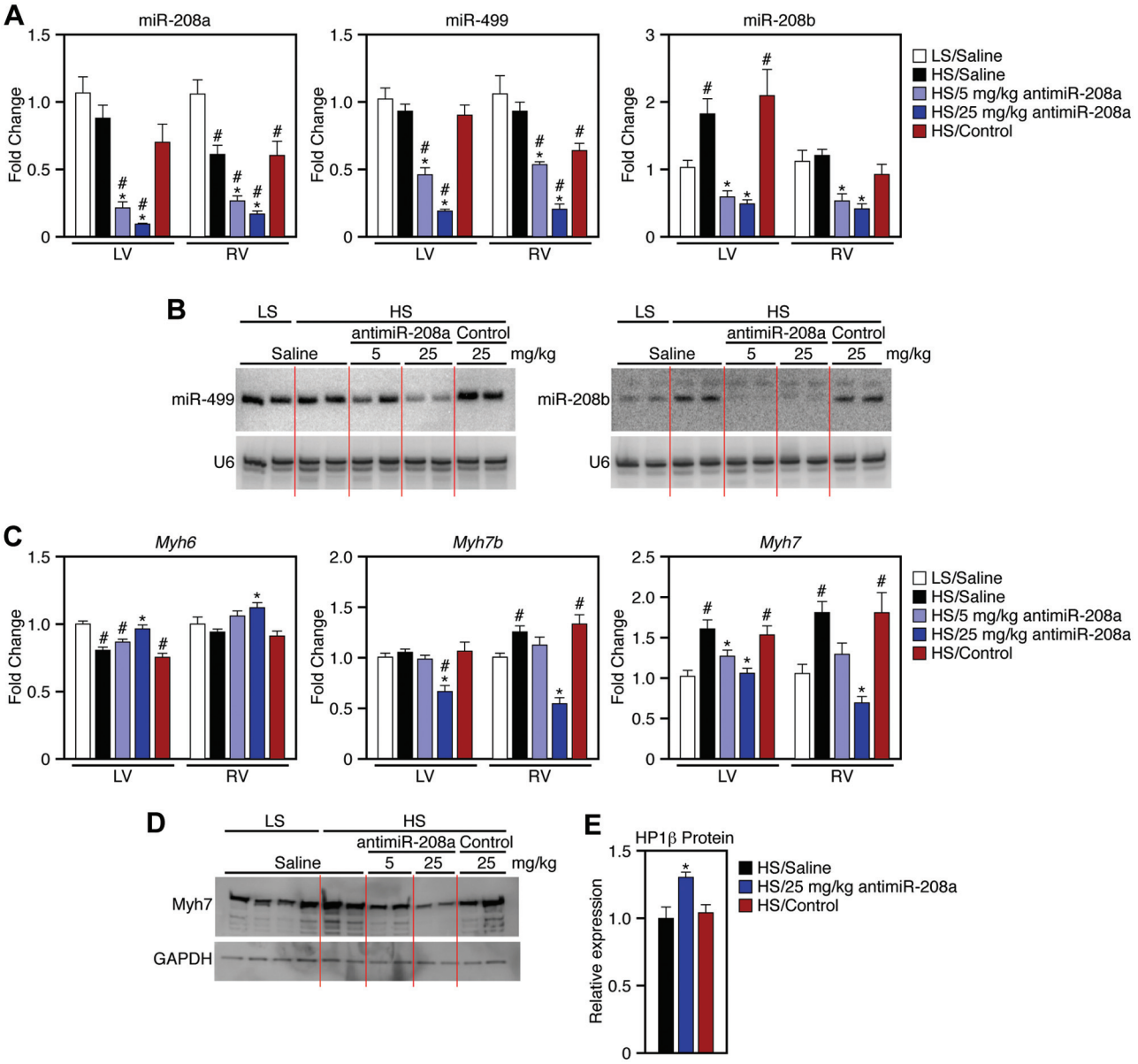

Figure 4. AntimiR-208a treatment reduces miR-499 and Myh7 in Dahl salt-sensitive rats. All analyses were performed 8 weeks after the start of a 4% high-salt (HS) diet and 7 weeks after the start of anti-miR treatment (n=10 for all groups in **A** and **C**). In **B** and **D**, each lane is a representative animal from the n=10 group. Rats were dosed every 2 weeks at 25 mg/kg (control) or the indicated dose of antimiR-208a starting 1 week after the HS diet. Red lines on graphs separate the groups. **A**, Real-time polymerase chain reaction analysis indicates a dose-dependent reduction of miR-208a in both the left ventricle (LV) and right ventricle (RV), which corresponds to a dose-dependent decrease in miR-499. Although miR-208b is increased in response to the HS diet, antimiR-208a significantly blunts this response. Administration of a scrambled control chemistry had no effect on the expression of miR-208a, miR-499, or miR-208b. **B**, Regulation of miR-499 and miR-208b in response to antimiR-208a treatment shown by Northern blot analysis. **C**, Real-time polymerase chain reaction analysis shows that the HS diet reduces *Myh6* and increases *Myh7*. AntimiR-208a treatment dose-dependently increases *Myh6* expression and reduces *Myh7b* expression. The HS diet–induced increase in *Myh7* is dose-dependently reduced by anti–miR-208a. **D**, Western blot analysis for Myh7 from ventricular tissue confirms the dose-dependent reduction in response to antimiR-208a treatment. GAPDH is used as a loading control. **E**, Quantification of HP1β Western blot showing miR-208a target derepression in the presence of antimiR-208a. The full blot in shown in Figure V in the online-only Data Supplement. In **A** and **C**, error bars depict the SEM. *$P<0.05$ vs HS/saline, #$P<0.05$ vs LS/saline.

AntimiR-208a Induces Specific Gene Expression Changes

Microarray analysis of hearts of Dahl rats on the HS diet that were injected with saline, antimiR-208a, or control oligo indicated that 131 genes were significantly changed in hearts of antimiR-208a–treated animals compared with control oligo–treated animals (Figure 5A and Table IV in the online-only Data Supplement). Only 15 genes (with a false-positive discovery rate of 67%) were significantly different between saline- and control oligo–injected animals, indicating that the LNA-modified oligos are highly specific in targeting miR-208a without any gene expression changes induced by the chemistry class (Figure 5A). Hierarchical clustering of the expression of the 131 sig-

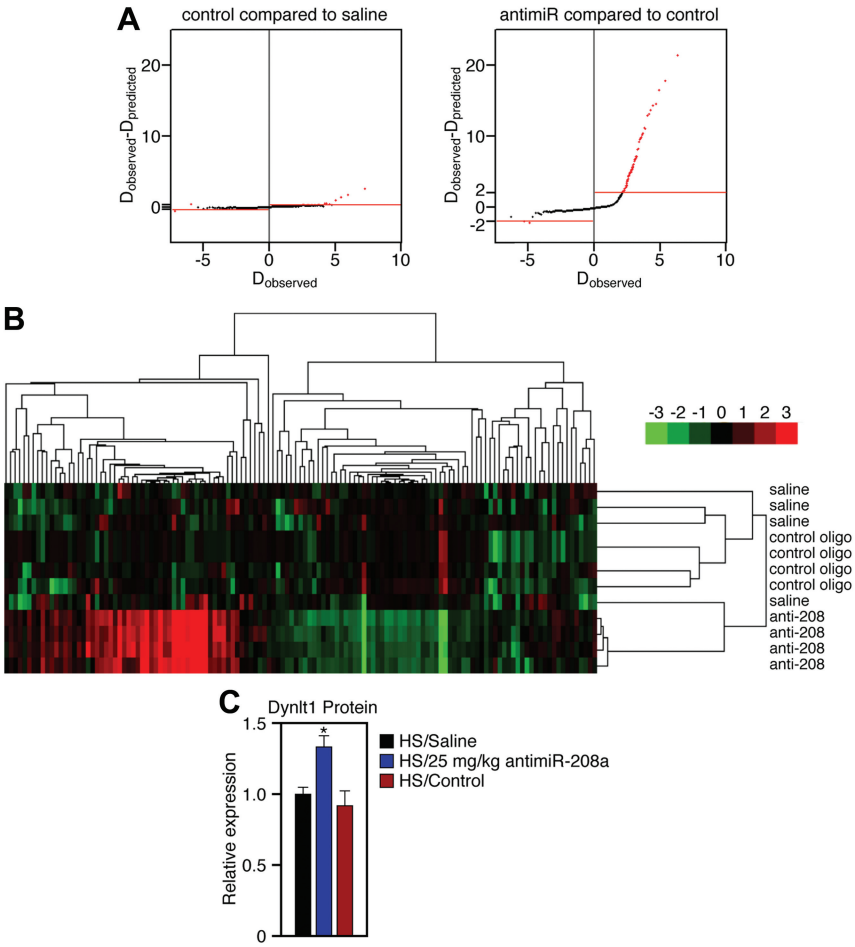

Figure 5. AntimiR-208a regulates a specific subset of genes in Dahl salt-sensitive rats. **A**, Microarray analysis was performed from left ventricular RNA from high salt (HS)/saline, HS/25 mg/kg antimiR-208a, and HS/control at 8 weeks after the start of a 4% HS diet and 7 weeks after the start of anti-miR treatment. Differential expression graphs show the numbers of genes that are differentially expressed when comparing gene expression in hearts of control-treated animals and saline-treated animals (left) or antimiR-208a–treated animals with control-treated animals (right). Dpredicted is the bioinformatically computed reference distribution for the 13 518 transcripts detected on the array. The transcripts highlighted in red are significantly different and due to nonrandom difference, as calculated by Dobserved-Dpredicted. **B**, Hierarchical clustering and heat map visualization of the 131 differentially expressed genes between control oligo– and antimiR-208a–treated hearts show clustering of treatment groups and few gene changes in the saline-treated vs the control oligo–treated animals. A full list of transcripts in given in Table IV in the online-only Data Supplement. **C**, Quantification of Dynlt1 Western blot showing miR-208a target derepression in the presence of antimiR-208a. A full blot in given in Figure VIII in the online-only Data Supplement.

nificantly changed genes between control oligo– and antimiR-208a–treated hearts showed robust clustering of upregulated and downregulated genes after antimiR-208a treatment (Figure 5B).

Gene array analysis confirmed the significant downregulation of *Myh7* and *Myh7b* in response to antimiR-208a compared with control oligo (-1.31, $P=0.005$; and -2.38, $P=0.037$, respectively). Of the 13 518 genes detected on the array, 289 rat genes were bioinformatically predicted to be miR-208 targets. Of these predicted targets, 28 genes showed increased expression with anti–miR-208 treatment by microarray ($P<0.05$), several of which were confirmed by real-time PCR (Figure VIII in the online-only Data Supplement). Upregulation of Dynlt1 was also confirmed by Western blot (Figure 5C and Figure IX in the online-only Data Supplement). Thirteen predicted targets showed decreased expression on the array ($P<0.05$). Seed enrichment analysis with a Kolmogorov-Smirnoff test showed a trend toward derepression of the seed-enriched targets but did not reach significance (data not shown). Because the gene expression analysis was performed on cardiac samples of animals that had been treated with saline, antimiR-208a, or control oligo for 8 weeks, we suspect the remainder of the gene expression changes to be secondary to the direct gene regulatory effects of miR-208a inhibition. BLAST analysis of the anti-miR sequence against the rat genome indicated that the sequence of antimiR-208a shows close homology (at least 14 bases of complementarity) to 4 coding sequences; however, none of these genes were regulated on the basis of microarray analysis.

miR-499 Is a Plasma Biomarker for AntimiR-208a Efficacy

Detection of miRNAs in plasma in various disease settings shows increasing diagnostic promise.[25] To determine whether there is a specific miRNA that correlates with antimiR-208a efficacy, we examined a panel of muscle-related miRNAs during HS treatment. Several muscle-specific miRNAs did not show significant differences between the groups tested (Figure X in the online-only Data Supplement). However, miR-499, although showing only modest increases in plasma detection under high salt, was significantly reduced in antimiR-208a–treated animals (Figure 6). Additionally, miR-423-5p plasma levels, which were previously correlated to human heart failure,[26] were found to be reduced in animals treated with antimiR-208a (Figure 6).

Discussion

The results of this study indicate that therapeutic inhibition of miR-208 leads to a reduction in cardiac remodeling, which coincides with a significant improvement in survival and cardiac function during heart disease.

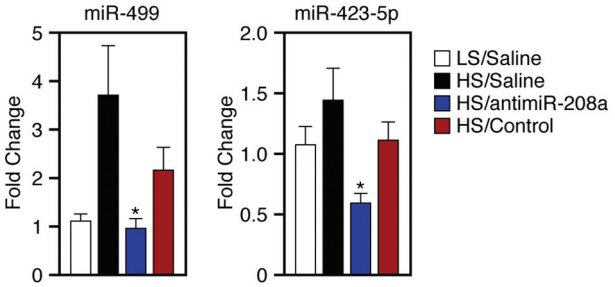

Figure 6. miR-499 in plasma serves a biomarker for antimiR-208a efficacy. Real-time polymerase chain reaction (PCR) analysis of the plasma samples indicates an increase in miR-499 in response to a high-salt (HS) diet, whereas antimiR-208a significantly lowers the detection of miR-499 in plasma 8 weeks after the start of a 4% HS diet and 7 weeks after the start of anti-miR treatment. Further miRNA analysis indicates a decrease in plasma-detectable miR-423–5p in response to antimiR-208a. *$P<0.05$ vs HS saline (n=10 per group).

Antisense oligonucleotides can be used to effectively silence miRNAs in vivo.[17–21] These anti-miRs are chemically modified to ensure in vivo stability, specificity, and high binding affinity to the miRNA of interest. A nucleic acid modification, LNA introduces a thermodynamically strong duplex formation with oligonucleotides while enhancing specificity toward complementary RNA or DNA.[17,18] Because of the high binding affinity, biological activity for LNA-modified anti-miRs is attained with shorter oligonucleotides (8–16 bases).[27] Recently, the therapeutic applicability of systemically delivered LNA-modified anti-miRs has been reported in nonhuman primates, in which inhibition of the liver-expressed miR-122 led to an improvement in hepatitis C virus–induced liver pathology in chronically infected chimpanzees.[21] Furthermore, it has recently been shown that anti-miR length can be altered, even down to 8 bases, with sustained inhibition.[28] We have tested additional lengths of anti-miRs; however, the 16-mer used here was the most efficacious in cardiac inhibition (data not shown). We believe that anti-miR length selection will be miRNA dependent, with A/U composition and copy number being factors.

A key finding in the present study is that systemic delivery of LNA-modified oligonucleotides is effective in inducing potent and sustained silencing of miR-208 in the heart. Sustained miR-208a inhibition and the absence of an effect on the closely related miR-208b, which differs by only 2 bp in the targeted region (Figure XI in the online-only Data Supplement), on systemic delivery of antimiR-208a indicate in vivo stability and specificity. We have further confirmed reciprocal specificity in which an anti-miR against miR-208b showed no miR-208a inhibition (data not shown). From the persistent miR-208a silencing and the downstream Myh7 regulation over time, it seems probable that antimiR-208a can accumulate in cardiac cells to silence all newly formed copies of miR-208a that are being produced by *Myh6* transcription. This effect might be reinforced further by the general lack of turnover of cardiomyocytes, preventing dilution owing to a decrease in the portion of cells that are targeted with the anti-miR.

Although gene regulatory effects of miRNAs on direct targets are fairly immediate, miR-208a inhibition requires several weeks before it establishes an effect on *Myh7b* and *Myh7* expression, as well as their intronic miRNAs, miR-499 and miR-208b, respectively. Although miR-208b and *Myh7* levels follow the same trend in downregulation, we recognize moderate differences in expression, which are likely due to stability differences and to differences in posttranscriptional regulation. We hypothesize that the delay in downstream biological effects is due to the requirement of alterations in the expression of many direct and indirect target genes of which the combined effects are required to induce the change. Given the modest and fine-tuning nature of miRNA regulation of many target genes, it likely takes some time to readjust the system after miRNA removal. miR-208 targets repressor proteins that are likely to contribute to Myh7 regulation and cardiac remodeling.[13] A comparable phenomenon was observed in response to miR-122 inhibition, which induces a lowering in plasma cholesterol, but not until several weeks after anti-miR treatment.[17,18] Nonetheless, the effect on Myh7b and Myh7 expression phenocopies the genetic deletion of miR-208a,[11,12] indicating that miR-208a is effectively silenced.

The therapeutic effects of antimiR-208a in the Dahl hypertensive rat provide strong evidence that subcutaneous delivery of LNA-based anti-miRs is sufficient to deliver anti-miRs effectively to the heart in vivo, and that miR-208a inhibition prevents cardiac remodeling, blunts functional deterioration, and delays lethality during heart disease. Currently, it remains unclear whether these effects arise solely from effects on cardiomyocytes as a result of miR-208a inhibition or whether there are extracardiac effects in response to miR-208a inhibition. However, the cardiomyocyte-specific expression of miR-208a, the dose responsiveness, and the absence of an effect in animals treated with a control chemistry strongly suggest that the observed effects are due to a lowering in miR-208a levels. Ongoing experiments will indicate whether this therapeutic benefit can be established in multiple models of heart failure.

Although the initial rodent data are encouraging and no adverse side effects were observed on anti-miR treatment, extensive analyses are required to determine the long-term safety of such agents in various settings. Comparable anti-miR chemistries are currently being evaluated in the first human clinical trials of miRNA inhibition (Santaris Pharma; www.clinicaltrials.gov).

Recently, miRNAs were detected in serum and plasma of humans and animals, suggesting the possibility of using miRNAs as diagnostic biomarkers of various diseases, including heart disease.[26,29–31] Plasma miRNA analysis shows that antimiR-208a treatment results in a diminution of miR-499 in blood serum, which parallels the decrease in cardiac expression of Myh7b/miR-499 in response to antimiR-208a treatment. Given the correlation between cardiac- and plasma-based miR-499 levels and the efficacy of antimiR-208a, these data suggest that plasma miR-499

levels might serve as a biomarker of effective delivery of antimiR-208a to the heart when moving into patients.

Myosin and subsequent MyomiR expression differs significantly between species. Whereas Myh6/miR-208a is the predominant myosin/MyomiR isoform in the hearts of rodents, larger mammals express more Myh7/miR208b.[16] Although miR-208a and miR-208b have overlapping seed sequence, they differ by 3 bases in their 3′ region (Figure VII in the online-only Data Supplement). Subsequent pharmacokinetic and efficacy studies in larger mammals are required to establish whether inhibition of miR-208a, miR-208b, or both is required to establish a comparable therapeutic effect in larger species. Additionally, because therapeutic use of miR-208 inhibition will likely be a combination therapy with current standard of care in heart failure patients, it will be important to assess whether antimiR-208a, in conjunction with current treatments, adds to the beneficial effects of these drugs. Taken together, this study demonstrates that subcutaneous delivery of LNA-based anti-miRs can effectively target the heart and further validates miR-208 as a target during cardiac disease.

Acknowledgments

We gratefully acknowledge our chemistry group for synthesis and purification of the oligonucleotides used in this study. We would like to express our gratitude to William Marshall for critically reading the manuscript. Additionally, we are thankful to Steve Lewton for technical assistance, Andreas Petri for help with bioinformatic analysis, and Jose Cabrera for graphics.

Sources of Funding

Work in Dr Olson's laboratory was supported by grants from the National Institutes of Health, Donald W. Reynolds Center for Clinical Cardiovascular Research, Foundation Leducq's Transatlantic Network of Excellence in Cardiovascular Research Program, American Heart Association–Jon Holden deHaan Foundation, and Robert A. Welch Foundation.

Disclosures

Drs Montgomery, Hullinger, Seto, and van Rooij, H.M. Semus, B.A. Dickinson, J.M. Lynch, C. Stack, and P.A. Latimer are employees of miRagen Therapeutics, Inc. Dr Olson holds equity in miRagen Therapeutics, Inc.

References

1. Hill JA, Olson EN. Cardiac plasticity. *N Engl J Med*. 2008;358:1370–1380.
2. Frey N, Katus HA, Olson EN, Hill JA. Hypertrophy of the heart: a new therapeutic target? *Circulation*. 2004;109:1580–1589.
3. Fatkin D, McConnell BK, Mudd JO, Semsarian C, Moskowitz IG, Schoen FJ, Giewat M, Seidman CE, Seidman JG. An abnormal Ca(2+) response in mutant sarcomere protein-mediated familial hypertrophic cardiomyopathy. *J Clin Invest*. 2000;106:1351–1359.
4. Gupta MP. Factors controlling cardiac myosin-isoform shift during hypertrophy and heart failure. *J Mol Cell Cardiol*. 2007;43:388–403.
5. Vanderheyden M, Mullens W, Delrue L, Goethals M, de Bruyne B, Wijns W, Geelen P, Verstreken S, Wellens F, Bartunek J. Myocardial gene expression in heart failure patients treated with cardiac resynchronization therapy responders versus nonresponders. *J Am Coll Cardiol*. 2008;51:129–136.
6. Lowes BD, Minobe W, Abraham WT, Rizeq MN, Bohlmeyer TJ, Quaife RA, Roden RL, Dutcher DL, Robertson AD, Voelkel NF, Badesch DB, Groves BM, Gilbert EM, Bristow MR. Changes in gene expression in the intact human heart: downregulation of alpha-myosin heavy chain in hypertrophied, failing ventricular myocardium. *J Clin Invest*. 1997;100:2315–2324.
7. Miyata S, Minobe W, Bristow MR, Leinwand LA. Myosin heavy chain isoform expression in the failing and nonfailing human heart. *Circ Res*. 2000;86:386–390.
8. Stelzer JE, Brickson SL, Locher MR, Moss RL. Role of myosin heavy chain composition in the stretch activation response of rat myocardium. *J Physiol*. 2007;579:161–173.
9. Small EM, Frost RJ, Olson EN. MicroRNAs add a new dimension to cardiovascular disease. *Circulation*. 2010;121:1022–1032.
10. Montgomery RL, van Rooij E. MicroRNA regulation as a therapeutic strategy for cardiovascular disease. *Curr Drug Targets*. 2010;11:936–942.
11. van Rooij E, Sutherland LB, Qi X, Richardson JA, Hill J, Olson EN. Control of stress-dependent cardiac growth and gene expression by a microRNA. *Science*. 2007;316:575–579.
12. Callis TE, Pandya K, Seok HY, Tang RH, Tatsuguchi M, Huang ZP, Chen JF, Deng Z, Gunn B, Shumate J, Willis MS, Selzman CH, Wang DZ. MicroRNA-208a is a regulator of cardiac hypertrophy and conduction in mice. *J Clin Invest*. 2009;119:2772–2786.
13. van Rooij E, Quiat D, Johnson BA, Sutherland LB, Qi X, Richardson JA, Kelm RJ Jr, Olson EN. A family of microRNAs encoded by myosin genes governs myosin expression and muscle performance. *Dev Cell*. 2009;17:662–673.
14. Berezikov E, Thuemmler F, van Laake LW, Kondova I, Bontrop R, Cuppen E, Plasterk RH. Diversity of microRNAs in human and chimpanzee brain. *Nat Genet*. 2006;38:1375–1377.
15. Landgraf P, Rusu M, Sheridan R, Sewer A, Iovino N, Aravin A, Pfeffer S, Rice A, Kamphorst AO, Landthaler M, Lin C, Socci ND, Hermida L, Fulci V, Chiaretti S, Foa R, Schliwka J, Fuchs U, Novosel A, Muller RU, Schermer B, Bissels U, Inman J, Phan Q, Chien M, Weir DB, Choksi R, De Vita G, Frezzetti D, Trompeter HI, Hornung V, Teng G, Hartmann G, Palkovits M, Di Lauro R, Wernet P, Macino G, Rogler CE, Nagle JW, Ju J, Papavasiliou FN, Benzing T, Lichter P, Tam W, Brownstein MJ, Bosio A, Borkhardt A, Russo JJ, Sander C, Zavolan M, Tuschl T. A mammalian microRNA expression atlas based on small RNA library sequencing. *Cell*. 2007;129:1401–1414.
16. van Rooij E, Liu N, Olson EN. MicroRNAs flex their muscles. *Trends Genet*. 2008;24:159–166.
17. Elmen J, Lindow M, Schutz S, Lawrence M, Petri A, Obad S, Lindholm M, Hedtjarn M, Hansen HF, Berger U, Gullans S, Kearney P, Sarnow P, Straarup EM, Kauppinen S. LNA-mediated microRNA silencing in non-human primates. *Nature*. 2008;452:896–899.
18. Elmen J, Lindow M, Silahtaroglu A, Bak M, Christensen M, Lind-Thomsen A, Hedtjarn M, Hansen JB, Hansen HF, Straarup EM, McCullagh K, Kearney P, Kauppinen S. Antagonism of microRNA-122 in mice by systemically administered LNA-antimiR leads to up-regulation of a large set of predicted target mRNAs in the liver. *Nucleic Acids Res*. 2008;36:1153–1162.
19. Krutzfeldt J, Kuwajima S, Braich R, Rajeev KG, Pena J, Tuschl T, Manoharan M, Stoffel M. Specificity, duplex degradation and subcellular localization of antagomirs. *Nucleic Acids Res*. 2007;35:2885–2892.
20. Krutzfeldt J, Rajewsky N, Braich R, Rajeev KG, Tuschl T, Manoharan M, Stoffel M. Silencing of microRNAs in vivo with "antagomirs." *Nature*. 2005;438:685–689.
21. Lanford RE, Hildebrandt-Eriksen ES, Petri A, Persson R, Lindow M, Munk ME, Kauppinen S, Orum H. Therapeutic silencing of microRNA-122 in primates with chronic hepatitis C virus infection. *Science*. 2010;327:198–201.
22. Hamalainen N, Pette D. Patterns of myosin isoforms in mammalian skeletal muscle fibres. *Microsc Res Tech*. 1995;30:381–389.
23. Shelton JM, Lee MH, Richardson JA, Patel SB. Microsomal triglyceride transfer protein expression during mouse development. *J Lipid Res*. 2000;41:532–537.
24. Rodenbaugh DW, Wang W, Davis J, Edwards T, Potter JD, Metzger JM. Parvalbumin isoforms differentially accelerate cardiac myocyte relaxation kinetics in an animal model of diastolic dysfunction. *Am J Physiol Heart Circ Physiol*. 2007;293:H1705–H1713.
25. Cortez MA, Calin GA. MicroRNA identification in plasma and serum: a new tool to diagnose and monitor diseases. *Expert Opin Biol Ther*. 2009;9:703–711.
26. Tijsen AJ, Creemers EE, Moerland PD, de Windt LJ, van der Wal AC, Kok WE, Pinto YM. Mir423–5p as a circulating biomarker for heart failure. *Circ Res*. 2010;106:1035–1039.

27. Petersen M, Wengel J. LNA: a versatile tool for therapeutics and genomics. *Trends Biotechnol*. 2003;21:74–81.
28. Obad S, dos Santos CO, Petri A, Heidenblad M, Broom O, Ruse C, Fu C, Lindow M, Stenvang J, Straarup EM, Hansen HF, Koch T, Pappin D, Hannon GJ, Kauppinen S. Silencing of microRNA families by seed-targeting tiny LNAs. *Nat Genet*. 2011;43:371–378.
29. Adachi T, Nakanishi M, Otsuka Y, Nishimura K, Hirokawa G, Goto Y, Nonogi H, Iwai N. Plasma microRNA 499 as a biomarker of acute myocardial infarction. *Clin Chem*. 2010;56:1183–1185.
30. D'Alessandra Y, Devanna P, Limana F, Straino S, Di Carlo A, Brambilla PG, Rubino M, Carena MC, Spazzafumo L, De Simone M, Micheli B, Biglioli P, Achilli F, Martelli F, Maggiolini S, Marenzi G, Pompilio G, Capogrossi MC. Circulating microRNAs are new and sensitive biomarkers of myocardial infarction. *Eur Heart J*. 2010;31:2765–2773.
31. Ji X, Takahashi R, Hiura Y, Hirokawa G, Fukushima Y, Iwai N. Plasma mir-208 as a biomarker of myocardial injury. *Clin Chem*. 2009;55:1944–1949.

CLINICAL PERSPECTIVE

Chronic and acute stress to the heart results in a pathological remodeling response accompanied by cardiomyocyte hypertrophy, fibrosis, pump failure, myocyte degeneration, and apoptosis, which often culminate in heart failure and sudden death. Although classic pharmacological treatment strategies can reduce remodeling and prolong survival in heart failure patients, these therapies are ultimately ineffective in preventing progression of the disease. Previously, we identified a microRNA, miR-208, encoded within an intron of the Myh6 gene that regulates the cardiac stress response. Although genetic deletion of miR-208 in mice failed to induce an overt phenotype at baseline, in response to several forms of cardiac stress, miR-208–null mice showed virtually no cardiomyocyte hypertrophy or fibrosis and were unable to upregulate Myh7 expression. Data presented in this study show that delivery of a locked nucleic acid–modified anti-miR against miR-208a in mice induces highly specific and sustained silencing of miR-208a in the heart without any observable side effects. Therapeutic silencing of miR-208a via subcutaneous delivery of antimiR-208a prevents pathological cardiac remodeling, functional deterioration, and lethality during heart disease. These beneficial effects correspond to significant changes in miRNAs within plasma. Our data show the potent beneficial effects of miR-208a inhibition, which could be very relevant for patients suffering from heart failure. Because miR-208a is the sole cardiac-specific miRNA annotated so far, we believe that antimiR-208a might become a combination therapy with the current standard of care.

SUPPLEMENTAL MATERIAL

Therapeutic inhibition of miR-208a improves cardiac function and survival during heart failure

Rusty L. Montgomery, PhD[1]; Thomas G. Hullinger, PhD[1]; Hillary M. Semus, BS[1]; Brent A. Dickinson, BS[1]; Anita G. Seto, PhD[1]; Joshua M. Lynch, BS[1]; Christianna Stack, MS[1]; Paul A. Latimer, BS[1]; Eric N. Olson, PhD[2]; and Eva van Rooij, PhD[1*]

[1]miRagen Therapeutics, 6200 Lookout Rd, Boulder, CO 80301; [2]Department of Molecular Biology, The University of Texas Southwestern Medical Center, 5323 Harry Hines Blvd., Dallas, TX 75390

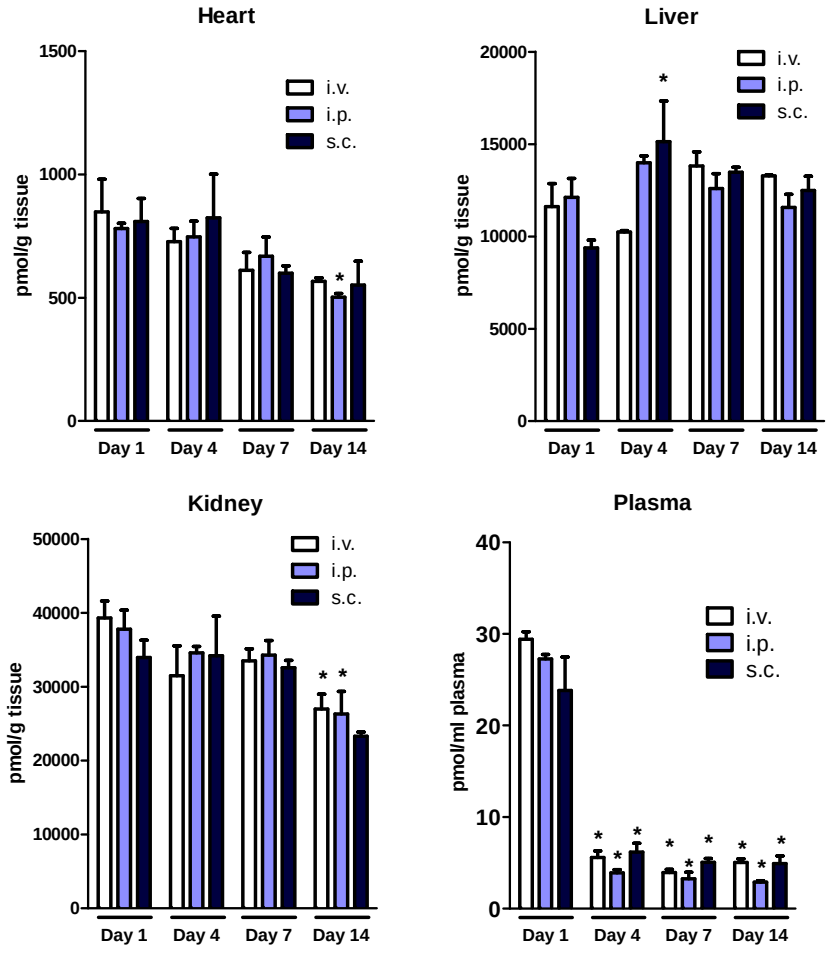

Supplemental figure 1. Plasma and tissue distribution data after antimiR-208a delivery. Mice were injected with a single dose of 25 mg/kg of antimiR-208 or saline, and sacrificed at the indicated time-points. Plasma and tissue distribution analysis indicates that comparable amounts of antimiR-208a are detectable by i.v, i.p. or s.c. delivery in plasma, heart, liver or kidney . Plasma detection significantly decreases after 1 day, while the tissue detection remains relatively constant. *$p<0.05$ vs. day 1, same route of administration. N=4 per group and time-point.

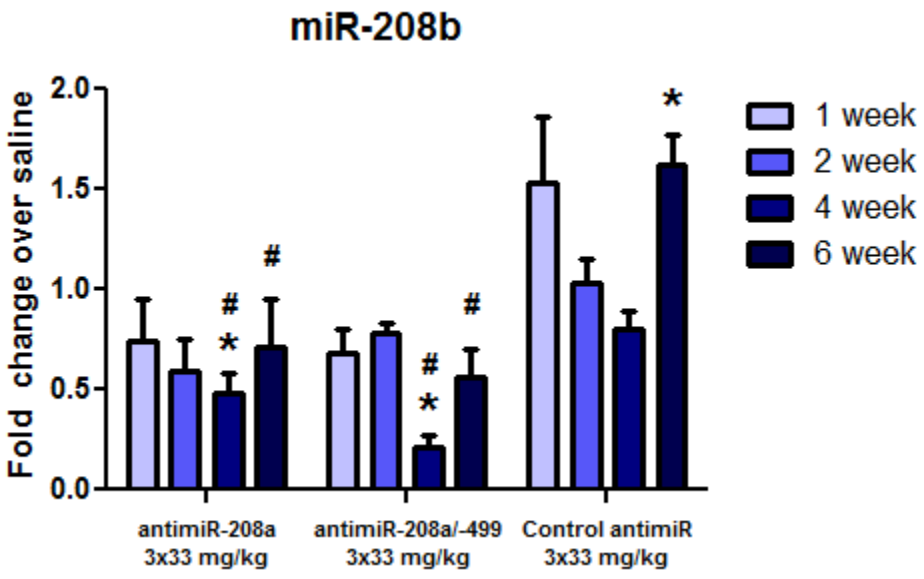

Supplemental figure 2. miR-208b expression in response to antimiRs. miR-208b expression is similar to that of its host gene, Myh7, showing down-regulation at 4 weeks and 6 weeks. Control antimiR does not show a robust effect on miR-208b expression. *p<0.05 vs. saline at the same time-point; #p<0.05 vs. control antimiR at the same time-point. N=4 per group and time-point.

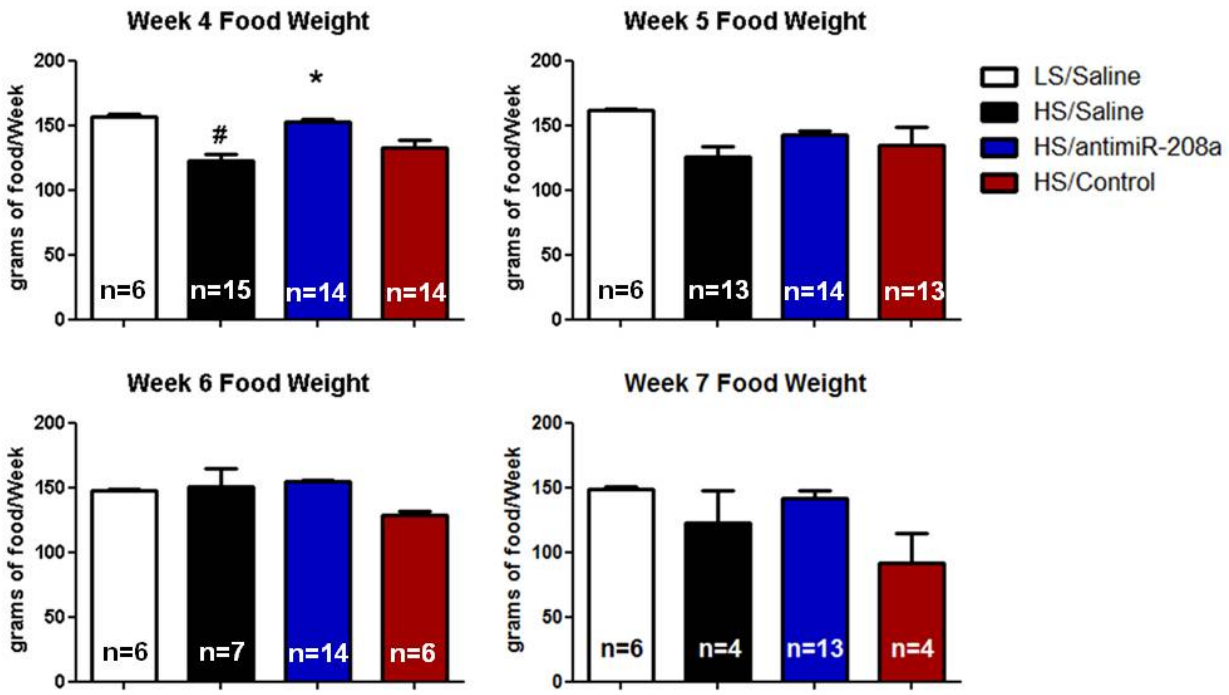

Supplemental figure 3. Food intake of Dahl salt-sensitive rats. Based on ingested amount of diet, there are no significant differences between the treatment groups, excluding the possibility that the differences in weight gain and health are due to differences in intake of the HS diet in the Dahl hypertensive rats. * $p<0.05$ vs. HS/Saline, # $p<0.05$ vs. LS/Saline

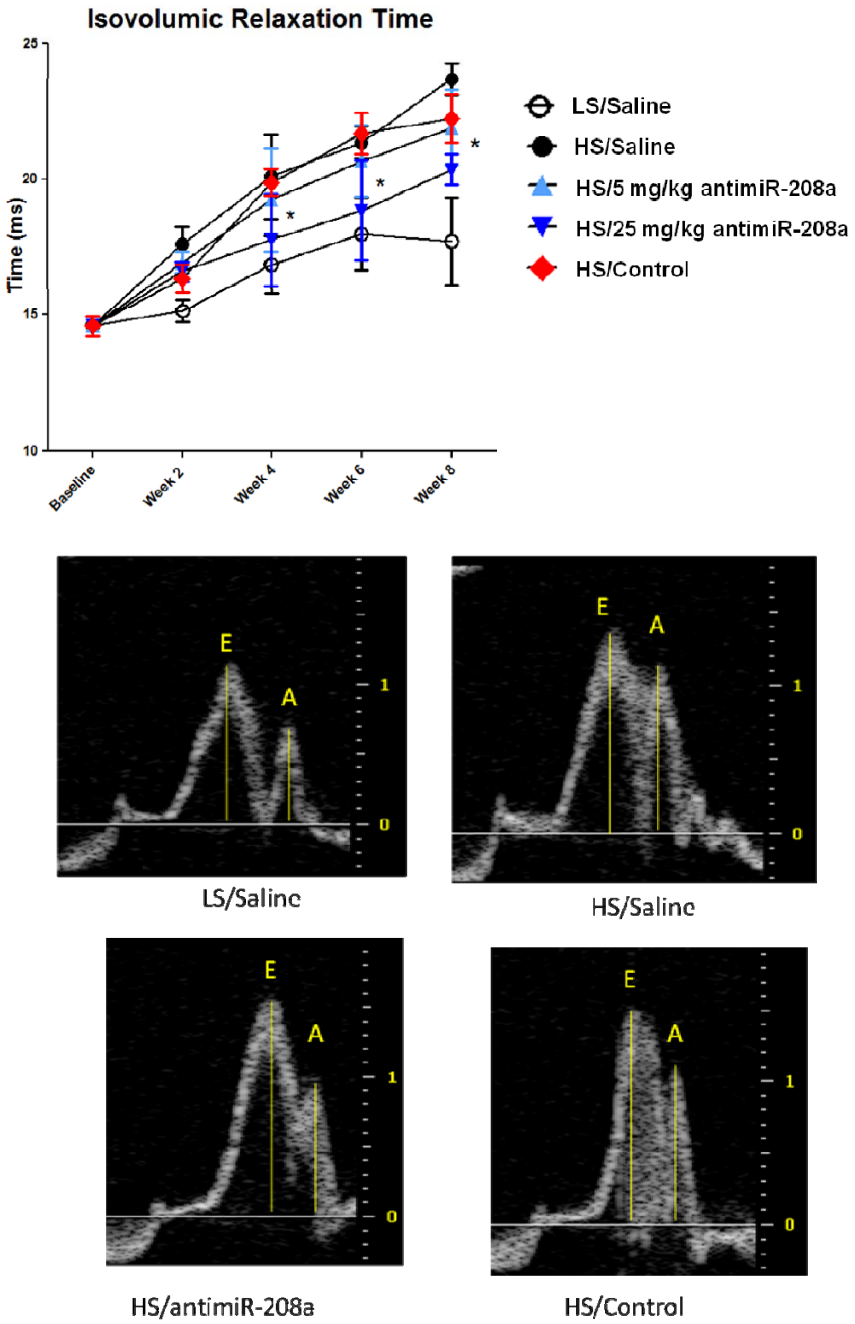

Supplemental Figure 4. (top) antimiR-208a treatment revealed a dose-dependent improvement in isovolumic relaxation time with 25 mg/kg resulting in a statistically significant decrease at weeks 4, 6 and 8 when compared to the HS saline group; whereas antimiR-208a at 5 mg/kg and the control at 25 mg/kg had no effect. (bottom) Representative doppler echocardiography images of mitral valve flow. The E and A waves are depicted. * ANOVA $p \leq 0.05$. N=10 per group.

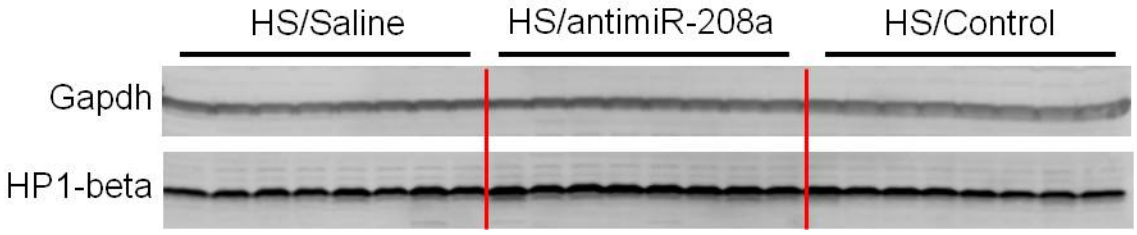

Supplemental figure 5. Western blot of HP1-beta in response to antimiR-208a. Western blot analysis of HP1-beta shows a de-repression in the presence of antimiR-208a. Quantification is Fig. 4E.

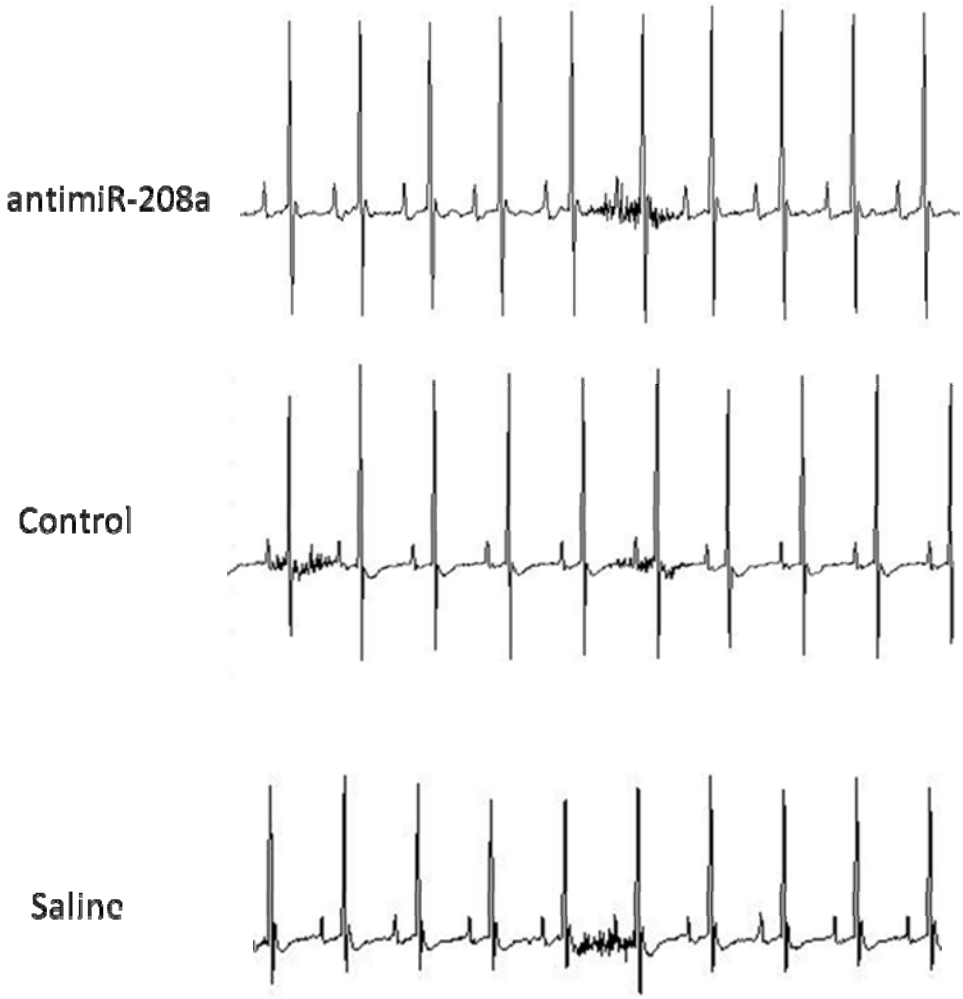

Supplementary figure 6. Representative ECG traces of mice treated with antimiR-208a or control oligo. ECGs were performed weekly and visually inspected for arrhythmias; none were observed. Small fluctuations that are seen are from breathing.

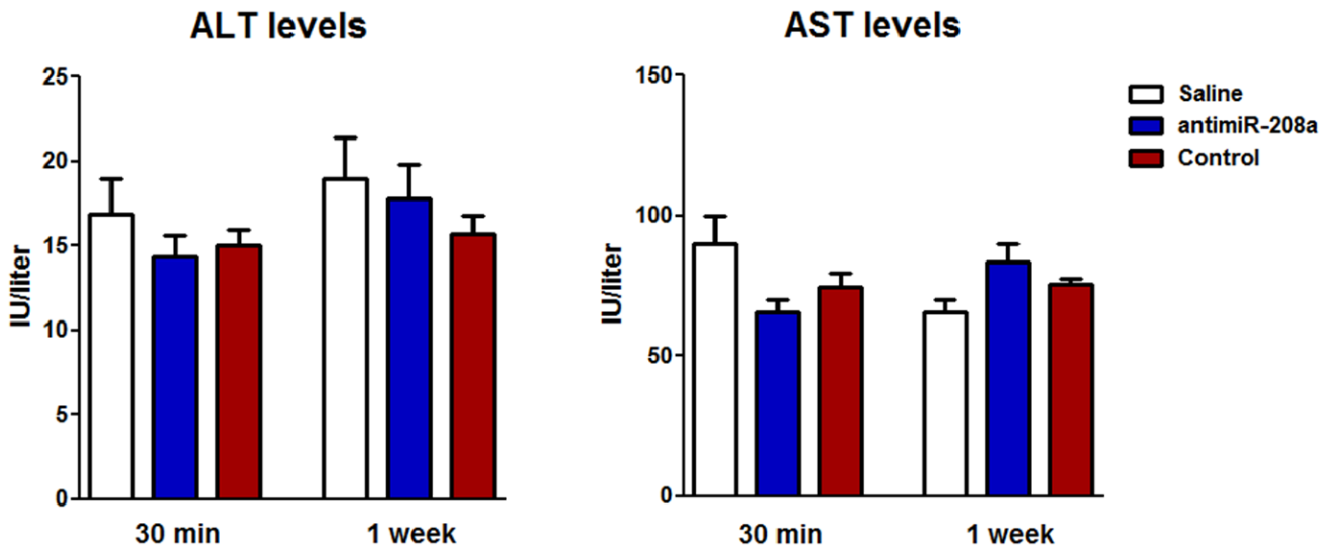

Supplemental figure 7. Detection of liver enzymes in response to antimiR-208a. Neither antimiR-208a nor control oligo treatment changed serum levels of the alanine aminotransferase (ALT) and aspartate aminotransferase (AST) liver enzymes in Sprague Dawley rats at 30 minutes or 1 week after 10 mg/kg i.v.dosing. N=4 per group.

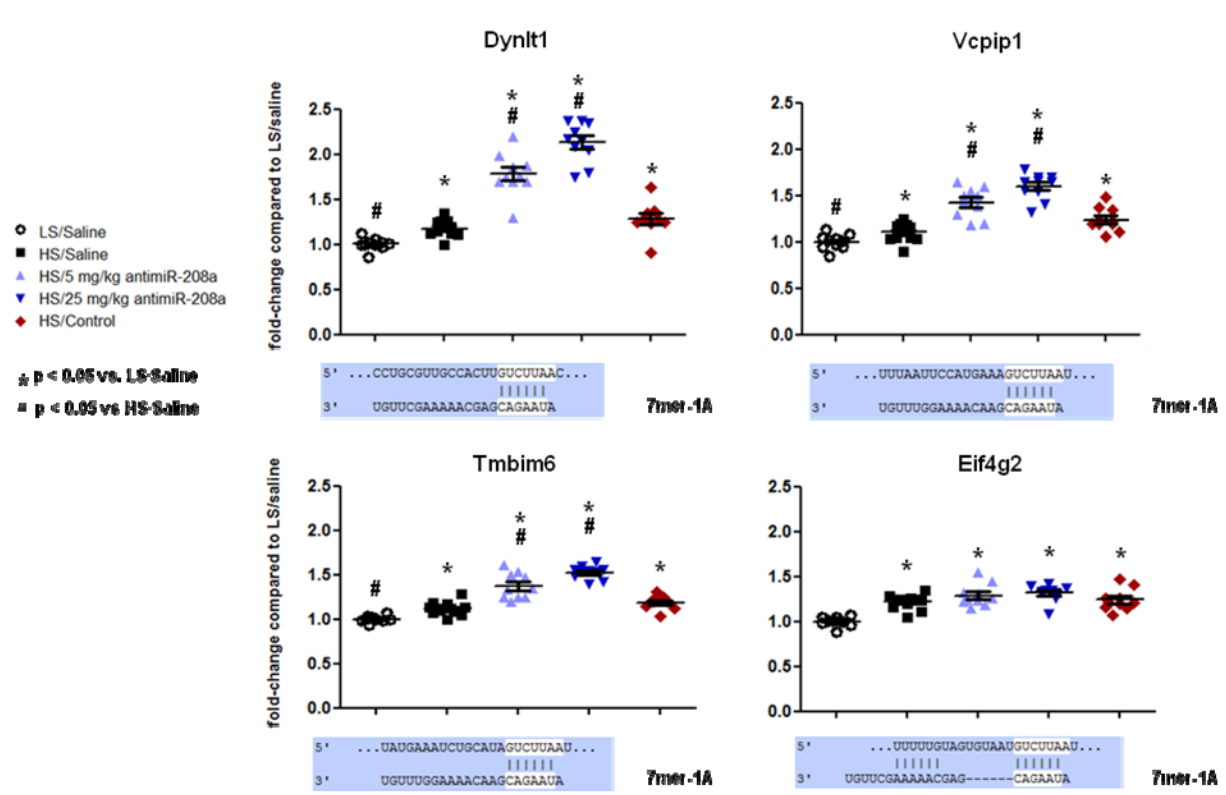

Supplemental figure 8. Expression changes in miR-208 targets. All analyses were performed 8 weeks following the onset of 4% HS diet and 7 weeks after the onset of antimiR treatment. Rats were dosed every two weeks at 25 mg/kg (control) or the indicated dose of antimiR-208a starting one week post-HS-diet. Real-time PCR analysis seven days after the last injection indicates a dose-dependent change in miR-208 targets in response to antimiR-208a treatment in 4% HS Dahl hypertensive rats while the control oligonucleotide has no effect. N=10 per group.

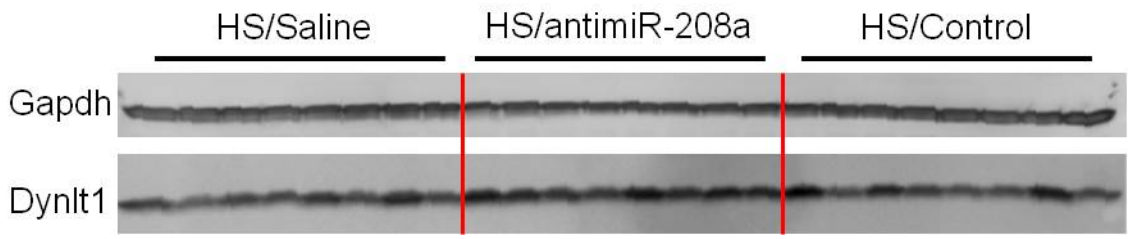

Supplemental figure 9. Western blot of Dnylt1 in response to antimiR-208a. Western blot analysis of Dnylt1 shows a de-repression in the presence of antimiR-208a. Quantification is Fig. 5C.

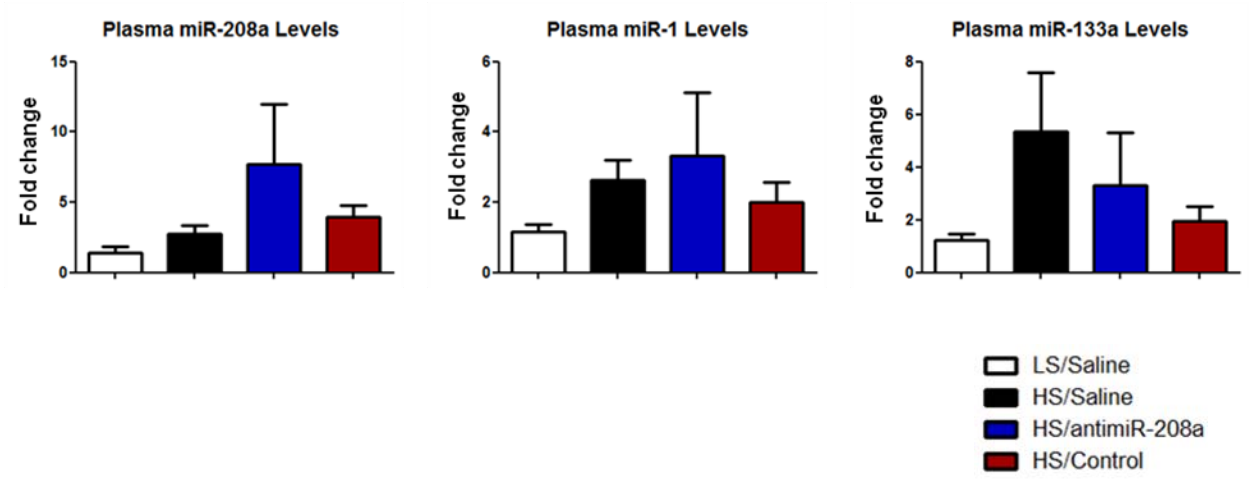

Supplemental figure 10. Plasma detection of muscle specific miRNAs. Plasma detection of several muscle-specific miRNAs shows no response to antimiR-208a treatment in Dahl hypertensive rats. N=10 per group.

Supplemental figure 11. MyomiR sequences. Mature sequences of miR-208a, miR-208b, and miR-499. Box indicates the seed region.

Group	HR (bpm)	PR (ms)	QRS (ms)	QT (ms)	QTc
Saline (n=4)	570.3 ± 12.2	36.32 ± 1.38	8.22 ± 0.29	45.83 ± 1.62	4.47 ± 0.17
Control (n=3)	543.2 ± 1.34	36.56 ± 0.24	8.82 ± 0.24	46.88 ± 1.24	4.46 ± 0.12
Anti-208 (n=4)	566.4 ± 19.9	34.67 ± 0.13	9.19 ± 0.44	45.33 ± 0.93	4.40 ± 0.09

Supplemental Table 1. Electrocardiogram parameters in response to antimiR-208a in mice. AntimiR-208a or comparable amounts of control oligonucleotide chemistry do not induce any signs of arrhythmias or improper cardiac conduction 6 weeks after repeated dosing of 25 mg/kg. Saline, n=4; Control, n=3; AntimiR-208a, n=4.

Group	HR (bpm)	PR (ms)	QRS (ms)	QT (ms)	QTc
LS/Saline (n=3)	416.9 ± 20.2	44.74 ± 2.48	16.06 ± 0.56	81.15 ± 4.38	6.74 ± 0.22
HS/Saline (n=3)	396.5 ± 17.3	47.98 ± 1.61	18.27 ± 1.43	100.1 ± 3.44 *	8.12 ± 0.11
HS/antimiR-208a (n=3)	420.2 ± 9.2	49.66 ± 1.23	17.96 ± 0.55	92.78 ± 3.60	7.76 ± 0.22
HS/Control (n=3)	404.6 ± 18.0	46.59 ± 2.06	17.24 ± 0.83	97.46 ± 4.96 *	7.25 ± 0.98

Supplemental Table 2. Electrocardiogram parameters in response to antimiR-208a in Dahl salt-sensitive rat. AntimiR-208a or comparable amounts of control oligonucleotide chemistry do not induce any signs of arrhythmias or improper cardiac conduction 8 weeks after biweekly dosing of 25 mg/kg in Dahl hypertensive rats. * $p < 0.05$ vs LS/Saline. LS/Saline, n=3; HS/Saline, n=3; HS/antimiR-208a, n=3; HS/Control, n=3.

Weights relative to body weight						
	HW	lungs	liver	spleen	r. kidney	l. kidney
saline	4.38 ± 0.10	6.32 ± 0.25	46.96 ± 1.24	1.85 ± 0.07	6.36 ± 0.35	6.12 ± 0.65
3 x 10 mg/kg antimiR-208a	4.68 ± 0.39	6.59 ± 0.55	51.21 ± 2.72	1.77 ± 0.02	6.66 ± 0.22	6.25 ± 0.62
3 x 10 mg/kg control	4.72 ± 0.46	6.55 ± 0.14	47.15 ± 4.54	2.24 ± 0.20	6.64 ± 0.67	6.35 ± 0.84
3 x 25 mg/kg antimiR-208a	4.41 ± 0.18	6.15 ± 0.27	47.97 ± 3.93	1.90 ± 0.21	5.82 ± 0.62	6.21 ± 0.47
3 x 25 mg/kg control	4.42 ± 0.09	6.76 ± 0.77	46.67 ± 6.46	2.38 ± 0.26	6.57 ± 0.44	6.75 ± 0.41

Supplemental Table 3. Mouse tissue weights in response to antimiR-208a treatment. AntimiR-208a or control oligonucleotide injections, either 3 x 10 mg/kg or 3 x 25 mg/kg, do not induce changes in mouse tissues weights 6 weeks after treatment. n=4 per group.

Transcript	Control Group Signal	antimiR-208a Group Signal	Est Log Ratio	Raw Est Fold Change	Delta (PADE)	FDR (PADE)	Individual Transcript p-value
Alox15	190.2	6.7	-4.84	-28.61	2.00	0.038	0.0001
Clcn2	9.9	1.9	-2.39	-5.23	2.00	0.038	0.0000
Dbh	7.5	1.8	-2.06	-4.18	2.00	0.038	0.0000
Actg (predicted)	788.9	1462.3	0.89	1.85	2.00	0.038	0.0000
Fcgrt	101.7	192.7	0.92	1.90	2.00	0.038	0.0001
Cln2	182.6	370.8	1.02	2.03	2.00	0.038	0.0001
Eef1a1	2088.2	4308.8	1.05	2.06	2.00	0.038	0.0001
Arpc5 (predicted)	285.0	592.5	1.06	2.08	2.00	0.038	0.0002
S100a6	154.8	321.7	1.06	2.08	2.00	0.038	0.0001
Spon1	35.9	78.5	1.13	2.19	2.00	0.038	0.0002
LOC310946	25.3	56.7	1.16	2.24	2.00	0.038	0.0002
Cap1	54.3	124.3	1.20	2.29	2.00	0.038	0.0000
Actb	1537.0	3535.2	1.20	2.30	2.00	0.038	0.0000
Stk17b	15.1	36.7	1.28	2.43	2.00	0.038	0.0004
Anxa4	169.8	413.6	1.28	2.44	2.00	0.038	0.0000
Ppgb (predicted)	124.3	304.3	1.29	2.45	2.00	0.038	0.0002
Ptpns1	115.4	283.0	1.29	2.45	2.00	0.038	0.0002
Pf4	139.0	345.0	1.31	2.48	2.00	0.038	0.0003
similar to 2310014H01Rik protein	18.1	45.7	1.34	2.52	2.00	0.038	0.0001
P2rx4	11.1	28.9	1.39	2.62	2.00	0.038	0.0002
Actb	616.7	1755.8	1.51	2.85	2.00	0.038	0.0000
Calcoco2 (predicted)	1.8	5.1	1.51	2.85	2.00	0.038	0.0001
Metrnl	41.6	118.9	1.52	2.86	2.00	0.038	0.0000
Ccl5	24.7	73.0	1.56	2.95	2.00	0.038	0.0006
Fnbp1l	60.3	179.4	1.57	2.97	2.00	0.038	0.0000
Ppt	123.4	368.5	1.58	2.99	2.00	0.038	0.0001
Arhgdib	177.3	537.5	1.60	3.03	2.00	0.038	0.0000
Tcirg1	26.8	81.3	1.60	3.04	2.00	0.038	0.0004
Murc (predicted)	1.4	4.5	1.68	3.21	2.00	0.038	0.0009
Maf	11.4	37.0	1.70	3.24	2.00	0.038	0.0000
RGD1564450	7.0	23.1	1.71	3.28	2.00	0.038	0.0003
similar to SIGLEC-like 1	1.6	5.3	1.72	3.30	2.00	0.038	0.0003
Ccr5	15.8	53.2	1.75	3.37	2.00	0.038	0.0008
Lgals3	183.8	638.8	1.80	3.48	2.00	0.038	0.0000
Smpdl3a	171.6	597.0	1.80	3.48	2.00	0.038	0.0000
Abcg1	43.3	151.3	1.80	3.49	2.00	0.038	0.0000
Myd88	9.2	33.6	1.88	3.67	2.00	0.038	0.0007

C7 (predicted)	13.3	50.3	1.92	3.78	2.00	0.038	0.0002
Lr8	35.5	139.6	1.98	3.93	2.00	0.038	0.0000
Ugt1a7	2.1	8.6	2.02	4.04	2.00	0.038	0.0013
similar to m33-A isoform	1.9	7.7	2.02	4.07	2.00	0.038	0.0011
Cd83 (predicted)	23.1	96.0	2.06	4.16	2.00	0.038	0.0009
similar to Tes	43.0	179.5	2.06	4.18	2.00	0.038	0.0000
Pfc (predicted)	22.0	99.0	2.17	4.50	2.00	0.038	0.0000
Cyba	210.2	1021.3	2.28	4.86	2.00	0.038	0.0000
Kif3b (predicted)	2.0	10.2	2.35	5.11	2.00	0.038	0.0013
Rhoh (predicted)	2.2	11.3	2.39	5.24	2.00	0.038	0.0015
Stap1 (predicted)	1.6	8.4	2.41	5.30	2.00	0.038	0.0009
Coro1a	19.5	103.7	2.41	5.32	2.00	0.038	0.0005
similar to immunoreceptor Ly49si1	2.7	14.6	2.43	5.40	2.00	0.038	0.0019
Irf5 (predicted)	1.8	10.0	2.45	5.45	2.00	0.038	0.0003
Trem2 (predicted)	30.5	167.4	2.46	5.49	2.00	0.038	0.0000
Cd44	2.2	12.4	2.47	5.55	2.00	0.038	0.0005
Cotl1 (predicted)	26.3	150.4	2.51	5.71	2.00	0.038	0.0000
Pltp (predicted)	196.0	1159.7	2.57	5.92	2.00	0.038	0.0000
Myo1f (predicted)	2.0	11.9	2.59	6.03	2.00	0.038	0.0015
C1qb	42.2	254.8	2.59	6.03	2.00	0.038	0.0000
similar to Fcgr2b	74.3	455.2	2.62	6.13	2.00	0.038	0.0000
Ctss	68.6	427.7	2.64	6.24	2.00	0.038	0.0004
Ptprc	1.4	8.4	2.64	6.24	2.00	0.038	0.0003
Arhgap9 (predicted)	4.3	27.6	2.69	6.46	2.00	0.038	0.0010
Plek (predicted)	7.5	48.5	2.70	6.48	2.00	0.038	0.0019
Rac2	79.0	524.2	2.73	6.63	2.00	0.038	0.0000
Tnfsf13	17.4	117.9	2.76	6.79	2.00	0.038	0.0005
Arl11 (predicted)	2.3	15.6	2.78	6.87	2.00	0.038	0.0005
Rarres1 (predicted)	1.7	11.6	2.82	7.04	2.00	0.038	0.0005
Pstpip1 (predicted)	1.6	11.4	2.82	7.06	2.00	0.038	0.0002
Apbb1ip (predicted)	1.2	9.0	2.91	7.54	2.00	0.038	0.0000
Lst1	2.7	20.9	2.96	7.75	2.00	0.038	0.0019
Pik3ap1 (predicted)	11.8	91.9	2.97	7.81	2.00	0.038	0.0000
C1qg	36.0	283.2	2.98	7.87	2.00	0.038	0.0000
Sart2 (predicted)	4.5	36.7	3.04	8.21	2.00	0.038	0.0000
C1qa	22.0	181.6	3.05	8.26	2.00	0.038	0.0013
Gpnmb	4.2	35.2	3.08	8.48	2.00	0.038	0.0007
Ncf4 (predicted)	2.1	17.9	3.10	8.58	2.00	0.038	0.0001
hypothetical gene supported by NM_016994	1.8	16.0	3.15	8.90	2.00	0.038	0.0000
Dcir2 (predicted)	1.3	11.3	3.16	8.91	2.00	0.038	0.0000
Inpp5d	1.8	16.3	3.18	9.04	2.00	0.038	0.0000
Hk3	1.6	14.6	3.20	9.17	2.00	0.038	0.0016
Basp1	3.8	35.6	3.21	9.26	2.00	0.038	0.0021

Unc93b (predicted)	2.6	24.4	3.24	9.44	2.00	0.038	0.0010
Igsf7	2.5	24.0	3.26	9.58	2.00	0.038	0.0021
Traf2 (predicted)	2.0	19.5	3.28	9.70	2.00	0.038	0.0012
Plcg2	2.3	22.9	3.32	9.96	2.00	0.038	0.0000
Laptm5	11.9	125.6	3.40	10.57	2.00	0.038	0.0009
Fam105a (predicted)	1.6	16.8	3.43	10.79	2.00	0.038	0.0004
Cd37	2.8	33.7	3.58	11.95	2.00	0.038	0.0011
Tyrobp	3.2	39.3	3.61	12.18	2.00	0.038	0.0008
Lcp1 (predicted)	70.9	895.8	3.66	12.64	2.00	0.038	0.0000
Bcl2a1	2.5	32.4	3.69	12.91	2.00	0.038	0.0007
Ptpro	5.9	77.0	3.70	12.95	2.00	0.038	0.0007
Gm2a	1.6	21.4	3.71	13.11	2.00	0.038	0.0001
similar to cell surface receptor FDFAC	2.5	33.0	3.72	13.18	2.00	0.038	0.0001
Dcir4	6.2	82.3	3.74	13.37	2.00	0.038	0.0004
Cybb	1.7	26.3	3.93	15.28	2.00	0.038	0.0000
Cd53	1.6	25.8	4.01	16.06	2.00	0.038	0.0000
similar to Fermt3	2.9	47.4	4.02	16.22	2.00	0.038	0.0014
Tnfsf13b (predicted)	1.7	28.0	4.08	16.85	2.00	0.038	0.0000
Slc11a1 (predicted)	1.7	30.2	4.14	17.58	2.00	0.038	0.0000
hypothetical LOC361349	1.7	30.3	4.18	18.06	2.00	0.038	0.0002
Fcgr3	1.1	20.3	4.20	18.34	2.00	0.038	0.0026
Cd68 (predicted)	13.0	241.0	4.21	18.49	2.00	0.038	0.0016
Aif1	73.4	1395.6	4.25	19.01	2.00	0.038	0.0000
Cd300le	2.2	43.1	4.27	19.32	2.00	0.038	0.0001
Ptpn6	6.5	127.8	4.30	19.67	2.00	0.038	0.0008
Ptprcap (predicted)	5.4	106.3	4.31	19.86	2.00	0.038	0.0003
Tnfrsf14 (predicted)	1.7	33.6	4.35	20.34	2.00	0.038	0.0000
Msr2 (predicted)	4.3	88.1	4.37	20.64	2.00	0.038	0.0006
similar to Immunoglobulin superfamily, member 7	1.2	24.1	4.37	20.66	2.00	0.038	0.0000
Lilrb3 (predicted)	2.1	45.3	4.40	21.17	2.00	0.038	0.0001
C6	1.9	39.2	4.41	21.19	2.00	0.038	0.0000
Tlr2	3.3	77.3	4.57	23.79	2.00	0.038	0.0001
Mrga10	1.9	46.1	4.60	24.30	2.00	0.038	0.0000
similar to NDUFS2	92.2	2377.0	4.69	25.79	2.00	0.038	0.0000
Glipr1 (predicted)	2.0	54.7	4.79	27.73	2.00	0.038	0.0000
Pld4 (predicted)	1.7	47.4	4.83	28.49	2.00	0.038	0.0001
Hem1 (predicted)	2.8	93.6	5.08	33.77	2.00	0.038	0.0000
Spn	6.2	217.9	5.13	34.97	2.00	0.038	0.0001
Tbxas1	1.5	54.3	5.21	37.01	2.00	0.038	0.0000
Ms4a7 (predicted)	7.8	296.8	5.25	38.07	2.00	0.038	0.0001
Emr1 (predicted)	1.7	76.0	5.49	44.93	2.00	0.038	0.0000
Folr2 (predicted)	1.7	93.9	5.75	53.78	2.00	0.038	0.0000
Naaa (predicted)	1.4	79.7	5.80	55.84	2.00	0.038	0.0000

Qprt	1.4	84.2	5.88	58.90	2.00	0.038	0.0000
Prkcb1	2.2	150.7	6.07	67.19	2.00	0.038	0.0000
Il18	2.0	169.9	6.43	86.38	2.00	0.038	0.0000
Slamf9 (predicted)	1.5	146.6	6.64	99.95	2.00	0.038	0.0000
Qprt (predicted)	1.2	165.0	7.06	133.60	2.00	0.038	0.0000
Dcir3 (predicted)	2.1	276.0	7.06	133.61	2.00	0.038	0.0000
Fcgr3a	1.8	1222.5	9.41	681.14	2.00	0.038	0.0000
Cxcl13 (predicted)	2.7	2802.4	10.00	1026.36	2.00	0.038	0.0000

Supplemental Table 4. List of 131 significantly regulated genes as shown in Figure 5.